EPRI | ELECTRIC POWER RESEARCH INSTITUTE

Radio Frequency Burn Mechanisms

Investigations into the Radiofrequency Burn Phenomenon

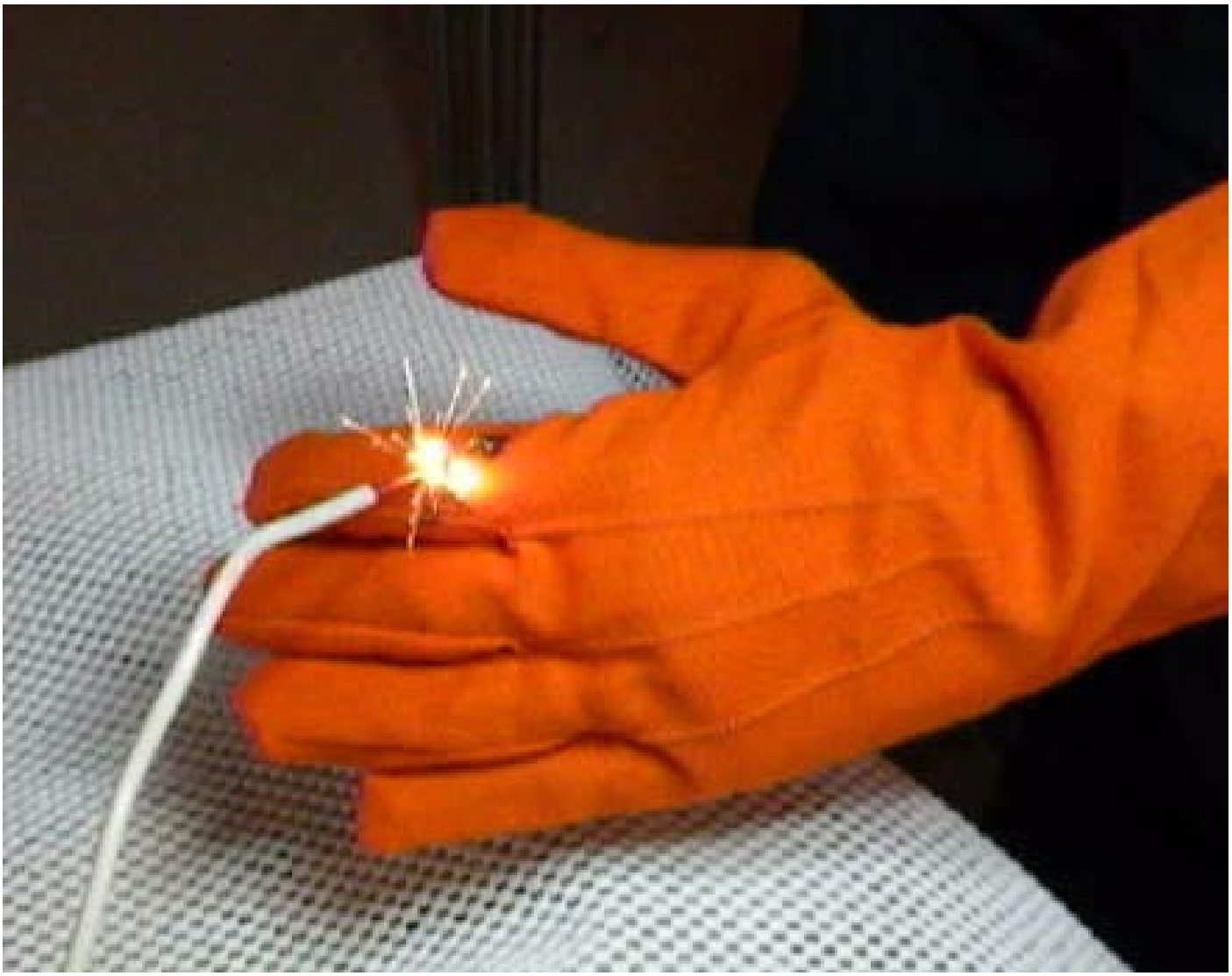

Cover photo: A 1.9 MHz electrical arc between a high voltage wire and a partially conductive glove used to offer some protection against the arc process. The glove material contains 12.5% stainless steel fibers in a matrix of Nomex™ fabric. (Photograph courtesy Richard Tell.)

Radio Frequency Burn Mechanisms

Investigations into the Radiofrequency Burn Phenomenon

1017991

Final Report, December 2009

EPRI Project Manager
R. Kavet
M. Silva

ELECTRIC POWER RESEARCH INSTITUTE
3420 Hillview Avenue, Palo Alto, California 94304-1338 • PO Box 10412, Palo Alto, California 94303-0813 • USA
800.313.3774 • 650.855.2121 • askepri@epri.com • www.epri.com

DISCLAIMER OF WARRANTIES AND LIMITATION OF LIABILITIES

ORGANIZATION(S) THAT PREPARED THIS DOCUMENT

Richard Tell Associates, Inc.

Washington State University

NOTE

For further information about EPRI, call the EPRI Customer Assistance Center at 800.313.3774 or e-mail askepri@epri.com.

CITATIONS

This report was prepared by

Richard Tell Associates, Inc.
1872 E. Hawthorne Avenue
Colville, WA 99114

Principal Investigator
R. Tell

Washington State University
College of Engineering
P.O. Box 642752
Pullman, WA 99164-2713

Principal Investigators
R. Olsen
J. Schneider

This report describes research sponsored by the Electric Power Research Institute (EPRI).

The report is a corporate document that should be cited in the literature in the following manner:

Radio Frequency Burn Mechanisms: Investigations into the Radiofrequency Burn Phenomenon. EPRI, Palo Alto, CA: 2009. 1017991.

PRODUCT DESCRIPTION

This report summarizes progress on understanding the nature and causes of radiofrequency (RF) burns. The research is intended to provide insights to hazards associated with RF burns as may be experienced with electric power system facilities.

Results & Findings

The report first provides background on what RF burns are, describes the experimental technical approach taken, and discusses test results. The report next examines RF burns at radio frequencies from contact with parasitically energized conductors via theoretical analysis. In following sections, the report discusses the problem as it exists in the continuous (real) world and then as it exists in the discretized (fields are available only at discrete points in space and time) world of the finite-difference time-domain (FDTD) method. Of primary significance, the report finds that open circuit voltages of 140 volts, traditionally taken as a threshold below which RF burns will not occur, is not protective. Additionally, contact currents specified in various standards to limit RF burns of 50 milliamperes also may not be protective. Additional work is indicated as appropriate to arrive at more definitive criteria to avoid RF burns.

Challenges & Objective(s)

The first topic addressed in this report concerns what exactly happens when a person comes into contact with a conductor that is energized either directly or parasitically with RF energy that may result in RF burns. The second topic examines the conditions under which maximum permissible exposures (MPEs) for electromagnetic fields are useful for protecting workers from intense currents injected in them (that may result in RF burns) while in contact with conductors indirectly energized by electromagnetic fields.

Applications, Values & Use

The project's primary goal is to identify conditions under which a significant RF burn can or cannot occur. Due to a lack of data, there are no standards for exposure to contact currents above 110 MHz that can cause RF burns. In this project, a model was developed to study RF burns at frequencies up to 500 MHz.

EPRI Perspective

Project results appear to support the concept that the maximum permissible exposure (MPE) may be protective against RF burns at frequencies higher than 110 MHz. However, questions about the level of detail needed in the human model are still open, and this conclusion must be treated as tentative. Present criteria commonly used to indicate the possibility of RF burns below 110 MHz may not be sufficiently protective.

Approach

An investigation of minimum open circuit voltages sufficient to initiate an electrical arc at radio frequencies was a high priority for the project team. With an emphasis on generating voltages of at least 140 volts rms, the team designed an apparatus that would permit evaluating the voltage required for an arc to occur between two electrodes. This voltage source was then used to explore the extent of electrical arcs that can occur between conductors. Using FDTD simulations where a man is approximated by the “average man” ellipsoid, the team was able to observe the effects on the amount of induced current when a parasitic element was in contact with the “average man.”

Keywords

Radio frequency
RF safety
RF burns
FDTD modeling

EXECUTIVE SUMMARY

The purpose of this report is to summarize progress on understanding the processes by and conditions under which radiofrequency (RF) burns can occur.

The first issue considered in this report concerns the question of what exactly happens when a person comes into contact with a conductor that is energized either directly or parasitically with RF energy. The purpose was to begin studying whether damage to the body occurs at the point of contact from an arc between the conductor and body just prior to contact and/or from excessive heat due to the injected current subsequent to contact. Given this information, the major goal is to determine the conditions (i.e., the open circuit voltage on a conductor prior to contact and/or the short circuit current from the contact point to an appropriate second terminal) that delineate between when a significant RF burn can or cannot occur. Based on the initial experiments performed in this ongoing study, the following conclusions can be made.

- The open circuit voltage of 140 volts used in IEEE Standard C95.1 – 2005 as a threshold for RF burns is probably not adequate to protect against damage from RF arcs and/or burns.
- The current of 50 mA used in Standard C95.1 – 2005 (for exposure in controlled environments) as a threshold for RF burns due to touch contact with a contact area of 1 cm^2 may not adequately protect against RF burns

Clearly, additional studies are needed to identify the specific conditions under which RF arcs and/or burns can occur. These studies are proceeding.

The second issue is to determine the conditions under which the "Maximum Permissible Exposures (MPEs)" for electromagnetic fields defined in several national and international RF Safety standards are useful for protecting workers from intense currents injected in them (and hence RF burns) while in contact with conductors indirectly energized by electromagnetic fields. Below approximately 50 MHz, it is well known that electromagnetic fields at amplitudes well below the MPE levels can cause RF burns under some circumstances when workers are in contact with large passive conductors. Thus, for this case it is necessary to develop separate criteria to protect against RF burns. This has been done in the standards by limiting the current injected into the body due to contact. Above approximately 50 MHz, it has been suggested that the MPEs may be protective against RF burns from contact with passive conductors in addition to hazardous biological effects. In fact, above 110 MHz, there are no standards for exposure to contact currents that can cause RF burns simply because of a lack of data. In the work reported here, a model has been developed and exercised to study RF burns at frequencies up to 500 MHz.

It can be concluded that: the results appear to support the concept that the MPE limit may be protective against RF burns at frequencies higher than 110 MHz. However, questions about the level of detail needed in the human model are still open and this conclusion must be treated as tentative.

CONTENTS

LIST OF FIGURES

LIST OF TABLES

1
INTRODUCTION

The purpose of this report is to summarize progress on understanding the processes by and conditions under which radiofrequency (RF) burns can occur. Of special interest are risks of RF burns that occur in the context of work on electric power system facilities. To this end, two research topics are reported here. These are introduced below.

The first research topic concerns the question of what exactly happens when a person comes into contact with a conductor that is energized (directly or parasitically) with RF energy. There is relatively little published information on this topic. This question is important for two reasons. First, it is not clear whether the most significant damage to the body occurs from an arc between the conductor and body just prior to contact or from excessive heat due to the injected current subsequent to contact. Of course, it is possible that both cause damage. Second (and dependent upon the answer to the first) the conditions that are protective of RF burns could relate to a threshold voltage if arc damage is important or steady state current if heat is the primary damage mechanism. To study this question, it is necessary to perform careful experiments so that the effects of the arc (when it exists) and the injected currents can be separated. In this case, the system designed to study these effects is a series resonant circuit (i.e., resistor, capacitor and inductor) that is driven by an RF transmitter. The voltage across the capacitor or the inductor can be used to generate an exposure that can cause both arcs and excessive temperature rises (i.e., burns). This report is a summary of the researcher's initial experiments and a description of the methodology to further study the RF burn phenomenon. The conditions under which arcs and significant thermal phenomena exist and which one causes the most significant damage will be studied by using a surrogate human skin model.

The second research topic concerns the "Maximum Permissible Exposures (MPEs)" for electromagnetic fields defined in several national and international RF Safety standards (e.g., Federal Communications Commission). These MPEs are designed to protect against hazardous biological effects due to RF electromagnetic field exposure. The question of whether or not the MPEs are also useful for protecting workers from intense currents injected in them (and hence RF burns) while in contact with passive conductors is the specific subject of this work. At frequencies below approximately 50 MHz, it has been observed that electromagnetic fields at amplitudes well below the MPE levels can cause RF burns under some circumstances when workers are in contact with passive conductors of large dimension. Thus, for this case it is necessary to develop separate criteria to protect against RF burns. This has been done in the standards by limiting the current injected into the body due to contact. Above approximately 50 MHz, however, the most recent research suggests that the MPEs may be protective against RF burns from contact with passive conductors in addition to hazardous biological effects above

some frequency (EPRI, 2008). In fact, above 110 MHz, there are no separate standards for exposure to contact currents that can cause RF burns. There is, however, a legitimate question about the validity of this conclusion since models that have been used to study RF burns are too crude to be used at frequencies above approximately 20 MHz. More specifically, the models treat the human as a simple two terminal impedance and hence ignore the direct interaction of the electromagnetic field with the human body. This is clearly not valid when the body becomes resonant and this can happen at frequencies as low as a few tens of MHz. The work reported in the first part of this section is original first work that fully models both the human body and the structure that is being contacted in a study of RF burns. More specifically, the model uses a standard model for the human body that has been used to develop RF exposure standards and a connected wire that "collects" energy from the field and delivers it to the body as a "contact current" at the point of contact between the body and wire. Thus, the model accounts for resonance effects in both the body and the contacted wire.

2
PRELIMINARY INVESTIGATION INTO THE NATURE OF RF BURNS

Background

Direct Interaction of Radiofrequency Electromagnetic fields with the Human Body

Radiofrequency (RF) exposure standards and regulations specify limits on the strength of RF fields to which individuals may be exposed. These limits control the rate of RF energy absorption within the body and, thereby, limit the extent of heating within the body as a whole and any particular part of the body from exposure to incident RF fields. Ironically, there are extremely limited reports in the medical and scientific literature that document adverse health effects that have resulted from exposure to RF fields exceeding various guidelines and standards. Nonetheless, monitoring and insuring that RF exposure of personnel complies with the relevant limits is an important aspect of RF safety programs.

Interference with Implanted Medical Devices

Just as RF fields lead to absorption of RF energy within the body's tissues, these same fields can lead to interference with the proper operation of medical electronic devices with the potential for subsequent adverse impact on the individual relying on the product.

RF Burns Due to Contact with Energized Objects

In addition to concerns over ambient RF fields and RF interference with electronic devices, the matter of RF burns presents itself as a definitive hazard to those who come into contact with objects that may act as sources of high RF voltages and currents. In fact, RF burns are arguably the most pronounced examples of RF hazards, yet are addressed with minimal detail in most RF exposure standards. The possibility of RF burns is presented anytime an individual touches an object, typically a conductor, which is energized (either directly or indirectly) with RF currents. The matter of just what level of energization is sufficient to produce an RF burn is the subject of this report.

Characteristics of RF Burns

RF burns are most easily characterized as the event that occurs when contact is made with a conductor, most often immersed in an RF electromagnetic field, that results in immediate and painful heating of tissue most commonly commensurate with visible skin damage and an involuntary reaction to withdraw from contact. The term burn is used to denote the sensation associated with more conventional burns. Conventional burns as well as RF burns are typically initiated at the surface of the skin but in the case of RF burns, tissue damage may extend immediately to deeper underlying tissue from high induced current densities. RF burns may be associated with an electrical arcing discharge that occurs between an object when relatively high RF voltage exists between it and the body. For example, the electric field produced by AM radio broadcast towers induces RF currents in the guy wires that support the antenna tower(s) and the high RF voltages found on these wires can often lead to small electrical arcs to the skin when a person initiates touching contact with the wire. At points where the arcing contacts the skin, just prior to physical contact, small, yellow or white burn spots can be produced on the skin. Alternatively (or in addition), an RF burn can occur when direct physical contact is made between the skin and an energized conductor so long as sufficient RF current is delivered to the point of contact with the body to result in tissue heating. A significant difference between these two mechanisms is that the former happens with extremely high localized current densities over very short duration exposure while the latter typically is associated with greater contact areas and lower current densities but such that the exposure duration before pain is sensed can be substantially greater than the arcing condition. The period of exposure before pain is experienced, however, is dependent on the magnitude of current that flows in the local tissue. If this current is sufficiently great, the burning sensation may occur almost instantaneously with little or no lag time. Limited reports in the scientific/medical literature have described cases of RF burns, e.g., Hocking et al.(1994); Hocking and Westerman (1999); Ciano et al.(1981).

Practical experience with RF burns reveals that, generally, the most troublesome form of burn occurs during momentary contact with a conductor, typical of a “dragging” contact, i.e., when the skin is not in solid contact with the conductor but, rather, there exists minute spacing between the skin and the conductor and the part of the body contacting the conductor makes intermittent contact. This process presents the opportunity for the skin to create “make” and “break” contact with the conductor which seems to exacerbate the presence of arcing. In practice, arcing is more probable during the “break” of a contact rather than the “make” of the contact. This is not to say that direct arcing between the energized conductor and the skin, just prior to contact does not happen. It certainly can but is dependent on the voltage difference between the skin and the conductor. Figure 2-1 is a close up photo of the surface of a human finger illustrating the irregular surface structure. When viewed on this microscopic scale, it is evident why the RF arcing phenomenon occurs during dragging contact as the ridges can make and break electric contact with the energized conductor. Figure 2-2 is an optical coherence tomography image of a finger tip with a scale to judge the physical dimensions of the skin ridges. This irregular surface will be seen to be highly relevant for the condition of intermittent and dragging contact with the surface of a high voltage source in that capacitive coupling between the source and the finger as well as direct physical contact can lead to extremely concentrated current densities in the subject and, hence, tiny burn points. This is not terribly dissimilar to the pitting process in relay contacts

whereby two presumably flat surfaces actually present microscopic high points known as "a spots" and which lead to contact surface erosion due to high localized current densities (Slade, 1999).

Figure 2-1
Close-up photograph of a human finger showing the many ridges that characterize the skin surface. Image reproduced with permission from Jim Ekstrom, Phillips Exeter Academy Science Department, Exeter, NH.

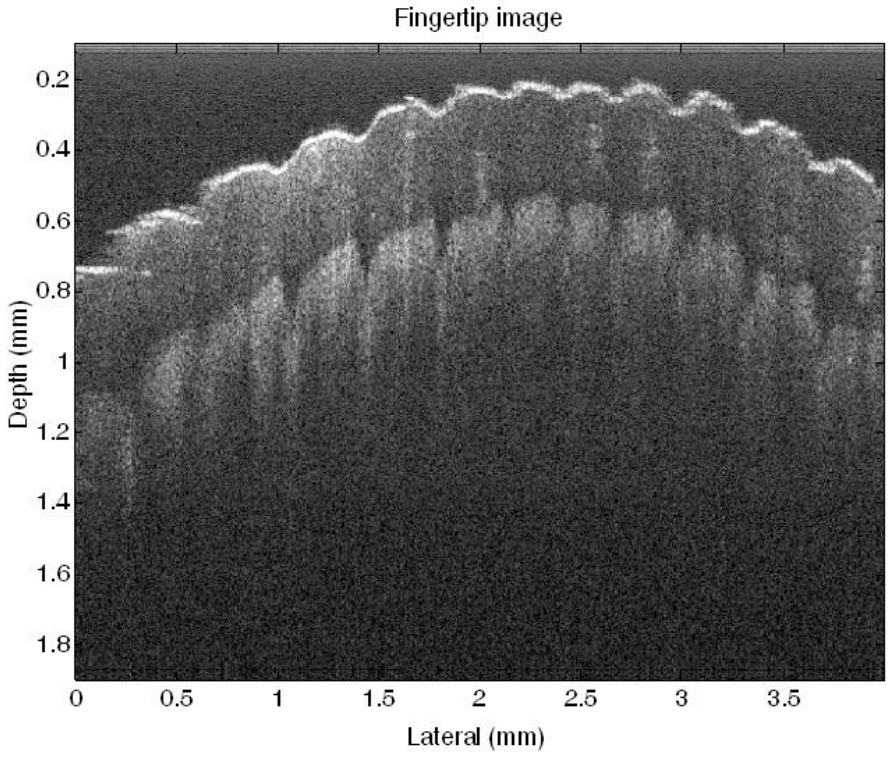

Figure 2-2
Functional optical coherence tomography image of a finger tip. Reproduced with permission from Professor Takashi Buma, Department of Electrical and Computer Engineering, University of Delaware.

Motivation for This Work

While RF burns have undoubtedly been recognized since the early days of radio, and represent clear hazards to workers who may receive such burns, relatively little research has been conducted on this topic compared with that on direct interaction of RF electromagnetic fields with the body (i.e., electromagnetic field energy absorption such as specific absorption rate (SAR) investigations). Whether this is a result of a perception that RF burns are less complex manifestations of RF interactions with the body is debatable. But it is universally recognized that RF burns are hazardous. Tissue destruction, even at minute points on the skin, can lead to infection that, if not treated, can result in adverse health effects. Further, despite direct health consequences of such burns, simply the startle reaction that is often accompanied with RF burns, along with the consequent implications in regard to accidents, is sufficient reason for avoiding and protecting against them.

RF burns can occur anytime contact is made with energized conductors whether the conductor represents an active element of an antenna used for communications (i.e., directly energized) or is simply an object that happens to be situated in an RF field that is sufficiently strong to induce high RF voltages and currents in the conductor (i.e., indirectly energized). For example, when work is performed near active transmit antennas, workers should avoid direct contact with bare element antennas. In the electrical utility industry context, linemen stringing new power

transmission lines near AM radio broadcast stations can be subject to substantial RF burn possibilities due to induced RF currents in the wires. Without an appreciation for the possibility of RF burns and the use of protective equipment such as insulated or conductive gloves, accidents can happen. But, interestingly, despite the recognition that RF burns may occur, little work has been accomplished to better understand the process of RF burns or to provide a quantitative approach to assessing exposure to this hazard.

Both the IEEE standard C95.1 (IEEE, 2005) and ICNIRP guidelines (ICNIRP, 1998) specify limits on induced body currents, currents that may flow within the body to ground, or between the body and other objects (contact currents). These limits were established, in the first place, to help control the local SAR in various regions of the body, particularly those with small conductive cross sections like the wrist and the ankle. In these documents, the recommended limits for contact currents vary over a relatively wide range being as low as 40 mA in the ICNIRP guidelines and as great as 100 mA in the IEEE standard, both specified as occupational limits. In an earlier issue of the IEEE standard (IEEE, 1999), the standard used language indicating that the contact current limits were "to prevent radio-frequency (RF) shock or burn…" and in the latest version of the IEEE standard (IEEE, 2005), it is stated that "In addition to the limits recommended for contact and induced currents, this standard also specifies an MPE for the open circuit voltage that exists on objects exposed to electric and magnetic fields in the frequency range of 0.1 to 100 MHz with which an individual may come into contact." Further, it states "The limits on induced RF currents are based on two different considerations. First, currents are limited to a level that protects against RF burns due to excessively high current densities in small areas of tissue while the subject is free standing in high-strength fields. These effects are much more pronounced and can occur at relatively low levels when one makes light, single-point contact with the object rather than rapid, grasping contact with the full hand." The IEEE standard suggests that measures of both the open circuit voltage on an object and the current that flows during contact may be needed to set criteria for RF burn hazards (Reilly, 1998).

These limits, for example 100 milliamperes (mA) for contact or 200 mA for induced body current through both feet to ground, are intended to prevent local SAR values from exceeding values specified within the IEEE standard. Localized SAR limits, however, contain averaging times of six-minutes and 30-minutes depending on whether the limits apply to occupational/controlled exposure environments or general public/uncontrolled exposure environments. Because of the rationale for limiting currents to limit local SAR, and because this is a heating phenomenon, the induced and contact currents have the same averaging times as the RF field MPEs, namely 6 minutes and 30 minutes for occupational and general public exposure respectively. Application of an averaging time allows the currents to increase and this carries with it the possibility of exacerbating any RF burn process that might occur. For example, in very small tissue volumes, similar to those that may be relevant in RF burns, high current values which correlate with the local energy absorption rates (SARs) could conceptually result in undesirable temperature elevations in very short exposure times. In an attempt to place some level of control on this possibility, a recent proposed amendment to the IEEE standard (IEEE, 2009), to correct its accidental deletion from the 2005 version, recommends ceiling values for induced and contact currents of 500 mA for occupational grasping contact. In application, this

means that a maximum of 500 mA is allowed to flow, during a grasping contact, for 15 seconds during any six-minute period. As will become evident, local tissue heating and the potential for an RF burn is highly related to the local current density that is developed when an individual comes into contact with an RF energized object. Hence, the surface contact area becomes a critical determinant of local heating rate and RF burn potential. This means that standards and guidelines that contain limits related to the control of RF burns must be interpreted with care since the values of contact currents may or may not be meaningful for a particular exposure condition.

The extent to which RF currents within body tissue can generate high rates of heating depends on the magnitude of the local current densities within the tissue and the current flowing within a tissue will be dependent on the voltage available to the tissue at the relevant contact points on the body, the appropriate impedance of the system that provides the current and the body impedance. Without sufficient voltage and small enough impedances, little current will flow. So, the issue of whether a sufficiently high value of current density exists within the tissue will also be related to RF voltage and relevant impedances. Hence, arriving at practical measures that can be used to predict the likelihood of an RF burn in different exposure scenarios can become complicated. While the value of current that ultimately flows within the tissue obviously determines the local energy absorption rate and, hence, tissue heating rate, it is important to be able to anticipate, prior to contact with objects, whether the current that will flow after contact can result in an RF burn. Identifying the measurement parameters that can best predict the potential for an RF burn becomes the challenge for this research. If the major hazard is related to the arcing phenomenon, just prior to physical contact with an energized conductor, then open circuit voltage on the conductor may be the most relevant parameter. But the impedance of the source (and the body) also will play a role in whether the voltage found on the conductor can deliver significant current to the body's tissue that will contact the object. If the RF burn phenomenon is purely related to thermalization of tissue, it may be that the energy associated with the spark that may occur prior to contact is not relevant. However, it also may be that the arc phenomenon may result in penetration of the skin and, hence, facilitation of a relatively lower conductivity path that results in a reduction in the apparent body impedance. These kinds of questions make the subject of RF burns intriguing from a technical perspective and have formed most of the basis for this project.

Past Work

Efforts to study RF burns have mostly been related to observational studies of individual's reactions to various currents flowing within the body, through the feet and at the point of contact. Rogers (1981) investigated RF currents as measured through the feet of individuals as they touched a 1.8 cm diameter conductive tube with the back of their index finger. In his work, volunteers touched the tube electrode that was energized with an RF power source and reported if they (a) could perceive the flow of current as represented by heating or (b) had an immediate painful reaction due to an RF burn.

Figure 2-3 illustrates data from Rogers (1981) for contact between the back of the forefinger and a 1.8 cm diameter brass tube. The ground connection was through the feet of the subject to a

large plate ground electrode. The study population was 50 persons, unidentified as to sex or age. Contact area on the finger has been estimated to be approximately 1.1 cm^2. Inspection of Figure 2-3 reveals that, apparently, some of the study participants could detect warming with 20 mA of RF current at 2 MHz. Generally, Rogers' data seem to indicate that at higher frequencies, the threshold current which could be detected increased.

Additional data from Rogers, as illustrated in Figure 2-4, provides evidence for the current that resulted in painful contact with the conductive tube electrode (described by Rogers as the "let go" current). In this test, with 50 individuals, the lowest let-go threshold was found, also, at 2 MHz with some individuals having to let go of the electrode at a current of 60 mA. If the contact area for this test was equivalent to approximately 1.1 cm^2, this would suggest that the let-go threshold surface current density was about 55 mA/cm^2.

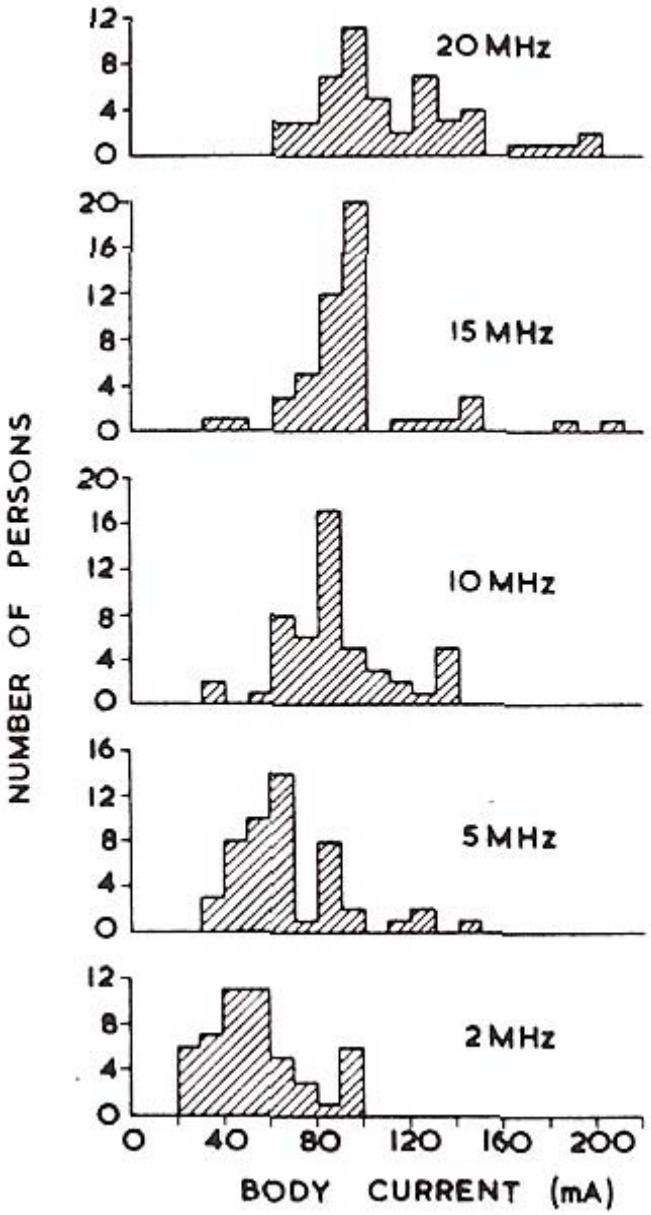

Figure 2-3
Perception current vs. frequency (Rogers, 1981).

Based on the human response data acquired by Rogers, he concluded that "an average hazard threshold current of 200 mA for the band 2-20 MHz" was appropriate with an additional observation that with grasping contact, currents of 500 mA or more could be drawn for short periods without discomfort. This value of 200 mA is found in the IEEE standard and cited as a basis for preventing RF burns.

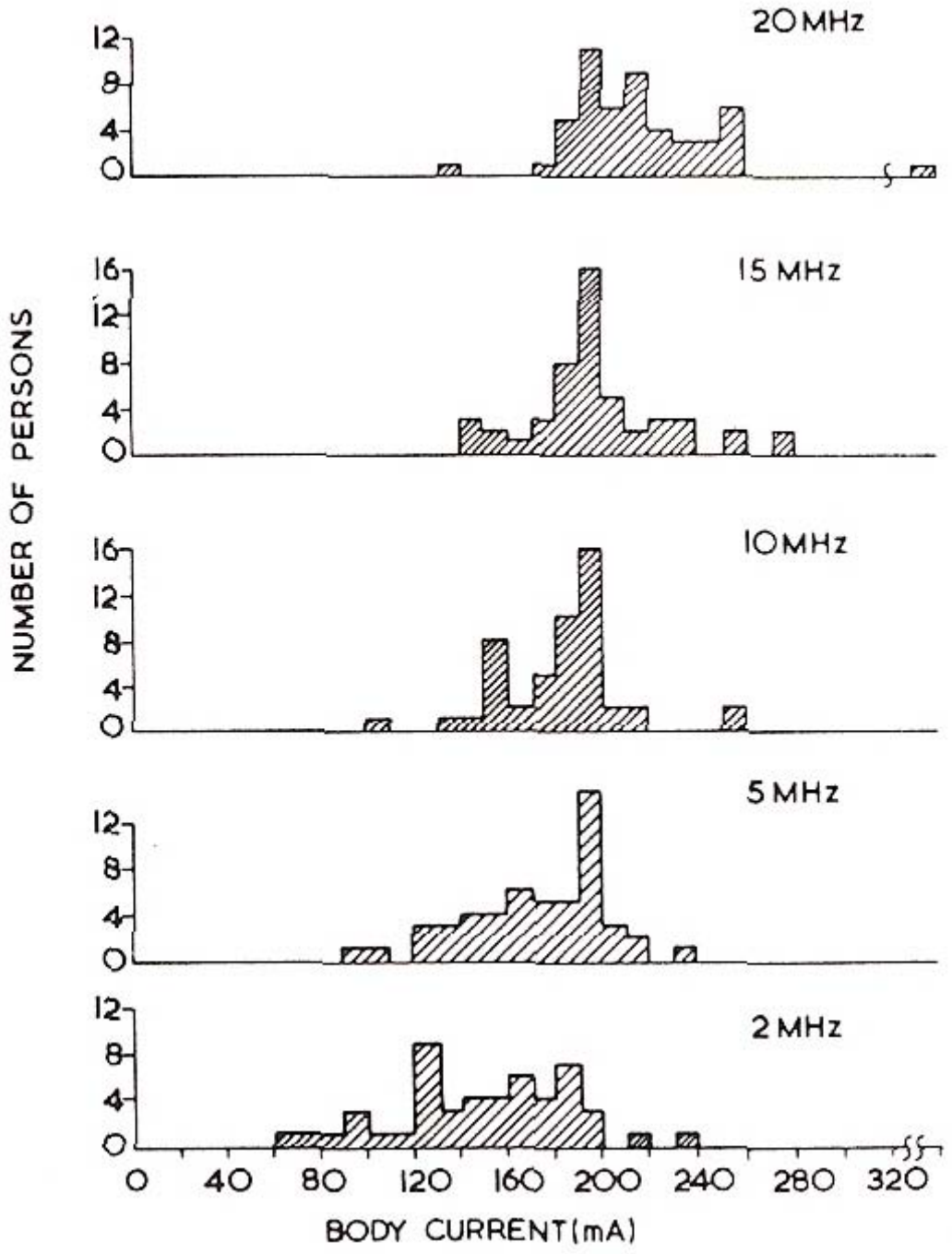

Figure 2-4
Let-go currents for 50 persons while touching the back of the forefinger to a 1.8 cm diameter conductive tube electrode (Rogers, 1981).

Exposure to ambient electric fields results in induced current in the body and these currents can been determined through calculations that have been established in the literature. For example, Gandhi et al. (1986) provided a formula for estimating the induced current that would flow to

ground through the feet for exposure to electric fields parallel to the standing body axis. Their formula, when expressed for a six-foot tall person is:

$$\frac{I}{E} = 0.361 f \left(\frac{mA}{V/m}\right) \qquad \textbf{(Equation 1)}$$

where
I is the induced body current in (mA)
E is the incident electric field strength (V/m)
f is the frequency (MHz)

This formula reveals that ambient electric fields that may be substantially less intense than the electric field MPEs in the IEEE standard or ICNIRP guidelines can result in induced currents that could significantly exceed the MPE for induced currents. As an example, at 30 MHz, which is near the upper frequency of 40 MHz for which Equation 1 applies, the induced current would be approximately 665 mA, well beyond the 200 mA induced current limit or the 100 mA contact current limit. Hence, compliance with the MPE does not, necessarily, imply compliance with the contact current limit and does not necessarily mean that the RF burn phenomenon can't happen. Nonetheless, Equation 1 allows for the estimation of currents that can be relevant to assessing the likelihood of RF burns.

Other research has studied the thermal perception of RF currents when flowing through the ankle and wrist. For example, Guy and Chou (1987) investigated leg currents that would result in measurable skin surface temperature increases in the very low frequency (VLF) band and high frequency (HF) band. These data were obtained by injecting RF currents into the leg and the arm using band-type electrodes placed around the leg and arm. Using data from Guy and Chou (1987), tissue current densities and local SARs were calculated by finding the average values from three temperature measurements on a male subject and three measurements on a female subject. The conductive cross section of the wrist is approximately 11.1 cm^2 (Gandhi et al., 1986; Chatterjee et al., 1986) while the bony aspect of the ankle results in a relatively small conductive cross section of only 9.5 cm^2 (Gandhi et al., 1986)[1]. Using an approximate cross section of 10 cm^2 for both the ankle and wrist, current densities associated with the rate of skin surface temperature rise and relative SAR were calculated and plotted in Figure 2-5.

[1] Note that there is some discrepancy in the presumed conductive cross section area of the ankle with some reports being in the range of 15 cm^2. Personal communication from S. G Allen to R. Tell conveying data from P. J. Dimbylow from the National Radiological Protection Board, UK (July 7, 1989).

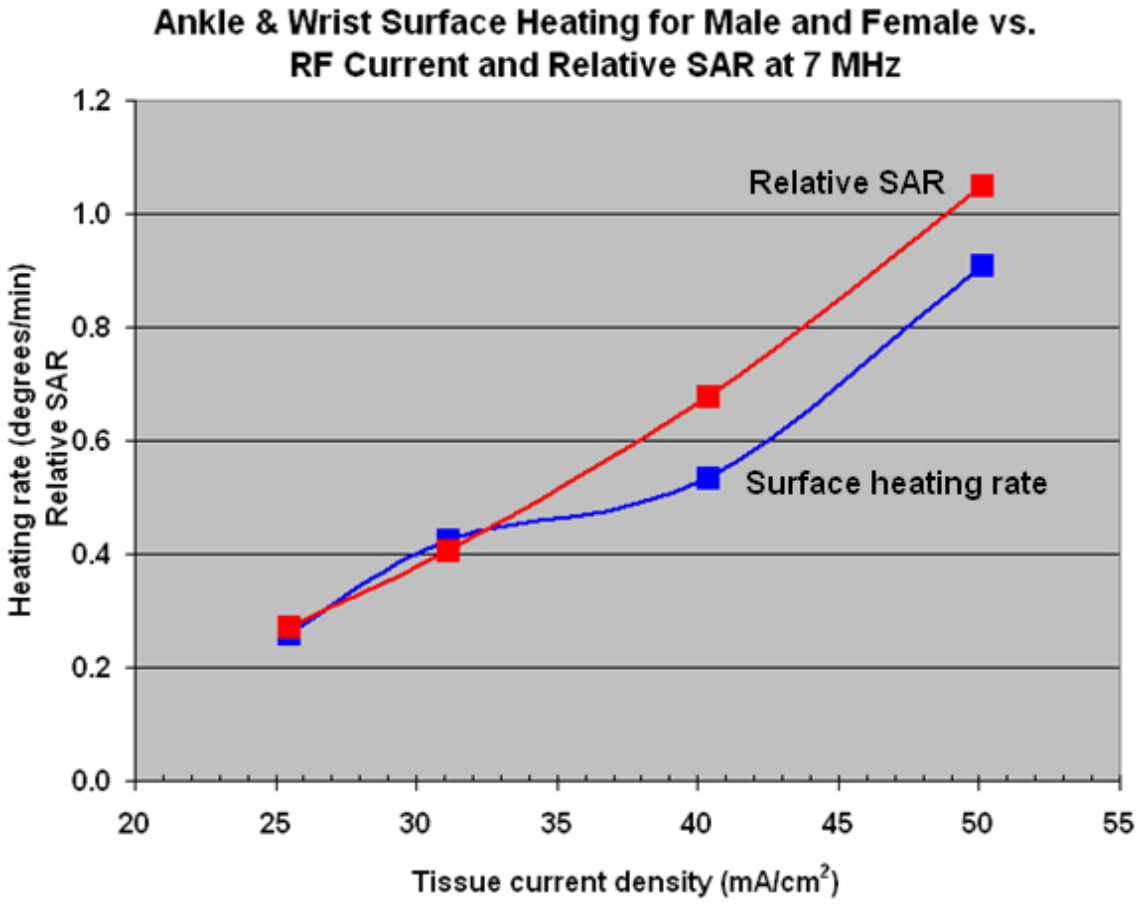

Figure 2-5
Analysis of data obtained by Guy and Chou (1987) on skin surface heating at the ankle and wrist with different RF currents injected at 7 MHz in a male and female subject. Three separate measurements of the surface temperatures were made in each case. Each data point represents an average of three male and three female temperature measurements. The relative SAR is also plotted based on current density and tissue conductivity.

The figure is illustrative of relatively large bulk tissue heating from RF currents at 7 MHz. Similar heating curves, within a factor of two, have been developed by Chen and Gandhi (1988) for surface heating of the ankle and wrist. In their work, they reported surface temperature elevations (ºC/min) equal to approximately 0.0047 x SAR with SAR expressed in watts per kilogram. Such data is interesting but is not especially relevant for the case of RF burns since, generally, RF burns are confined to rather small parts of the anatomy with local current densities or SARs that greatly exceed the body's ability to dissipate the heat in an effective manner.

Of more relevance to the problem of RF burns, which always start at the skin surface, is the temperature duration of heating that can result in pain and skin necrosis. A summary of thermal threshold data for tissue damage is provided by Dewhirst et al. (2003). The authors made use of work performed by Moritz and Henriques (1947) and Stoll and Greene (1959). Figure 2-6 provides the human data showing the time to result in various biological endpoints (isoeffects) as a function of temperature. Of particular relevance is the curve showing pain (the lower curve in

the figure) and the curve for skin necrosis. The data indicate that a temperature of approximately 45 ºC for 12 seconds and approximately 48 ºC for 2 seconds was found to elicit a painful reaction with a likely "almost instantaneous" pain threshold of about 50ºC. Skin necrosis was observed to occur at a temperature of 60ºC for approximately 5 seconds.

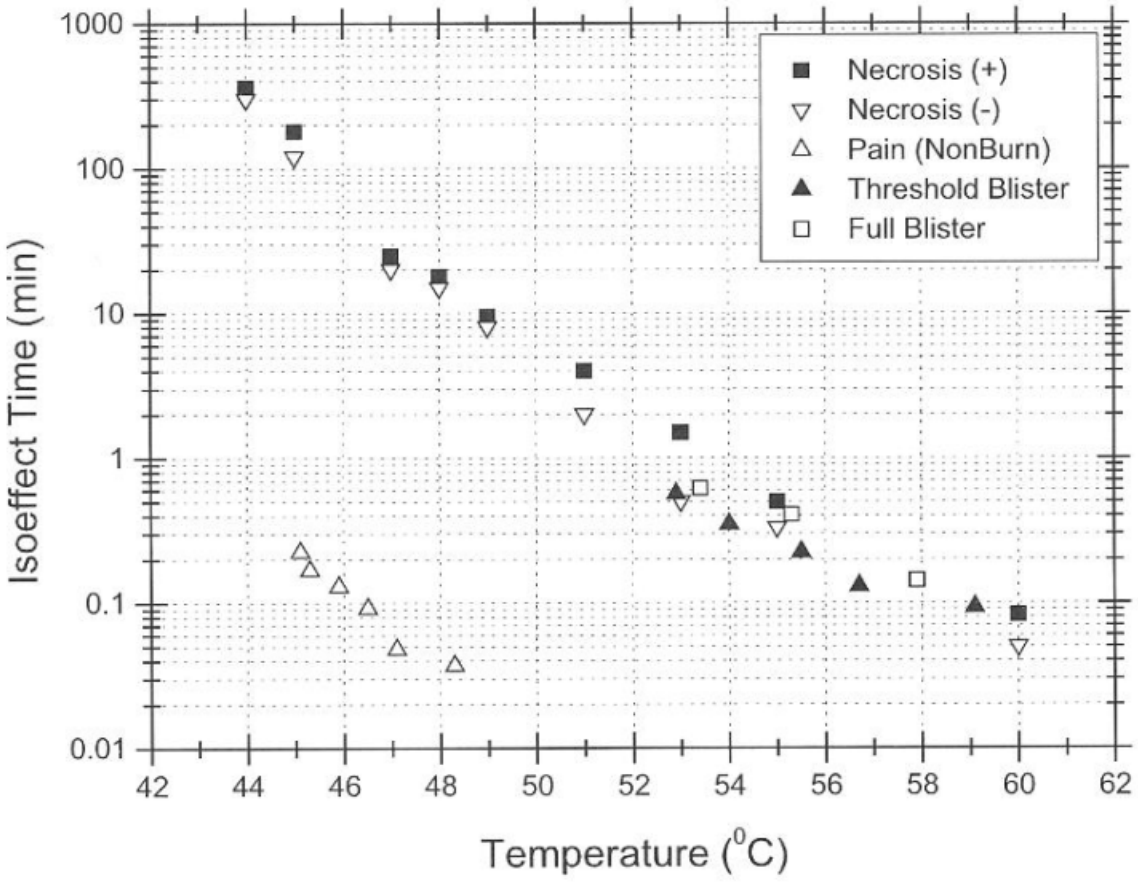

Figure 2-6
Time-temperature combinations to achieve varying thresholds of thermal damage to human skin. Figure reproduced from (Dewhirst et al., 2003, Figure 3a) under license 2303201174494 with Taylor and Francis. Note that the pain threshold is significantly lower than the threshold for significant injury.

The ability of persons to perceive the flow of RF currents in the VLF and MF bands was investigated by Chatterjee et al. (1986). Test results for perception when touching the front of the finger contact with the plate electrode of area 25 mm^2 are presented in Figure 2-7. In this figure, the threshold for just perceiving current flow was observed to increase with frequency to approximately 100 kHz after which the threshold was found to remain relatively constant with frequency up to the limit of the test at 3 MHz. 100 kHz is often taken as the boundary below which neurostimulatory effects predominate and above which the effect is tissue heating. Above 100 kHz, the perception current thresholds were found to be approximately 44 mA for males, 37 mA for females and 25 mA for children. In similar experiments to evaluate pain thresholds, again for front of finger contact with the plate electrode, the thresholds were 53 mA for males,

47 mA for females and 33 mA for children (see Figure 2-8). In separate experiments, the authors noted that the threshold currents above 100 kHz for perception with finger contact with a larger, 144 mm^2 plate were approximately 1.5 times the values obtained with the smaller plate. They concluded that perception was dependent on a threshold current density for the sensation of heat/warmth at the higher frequencies.

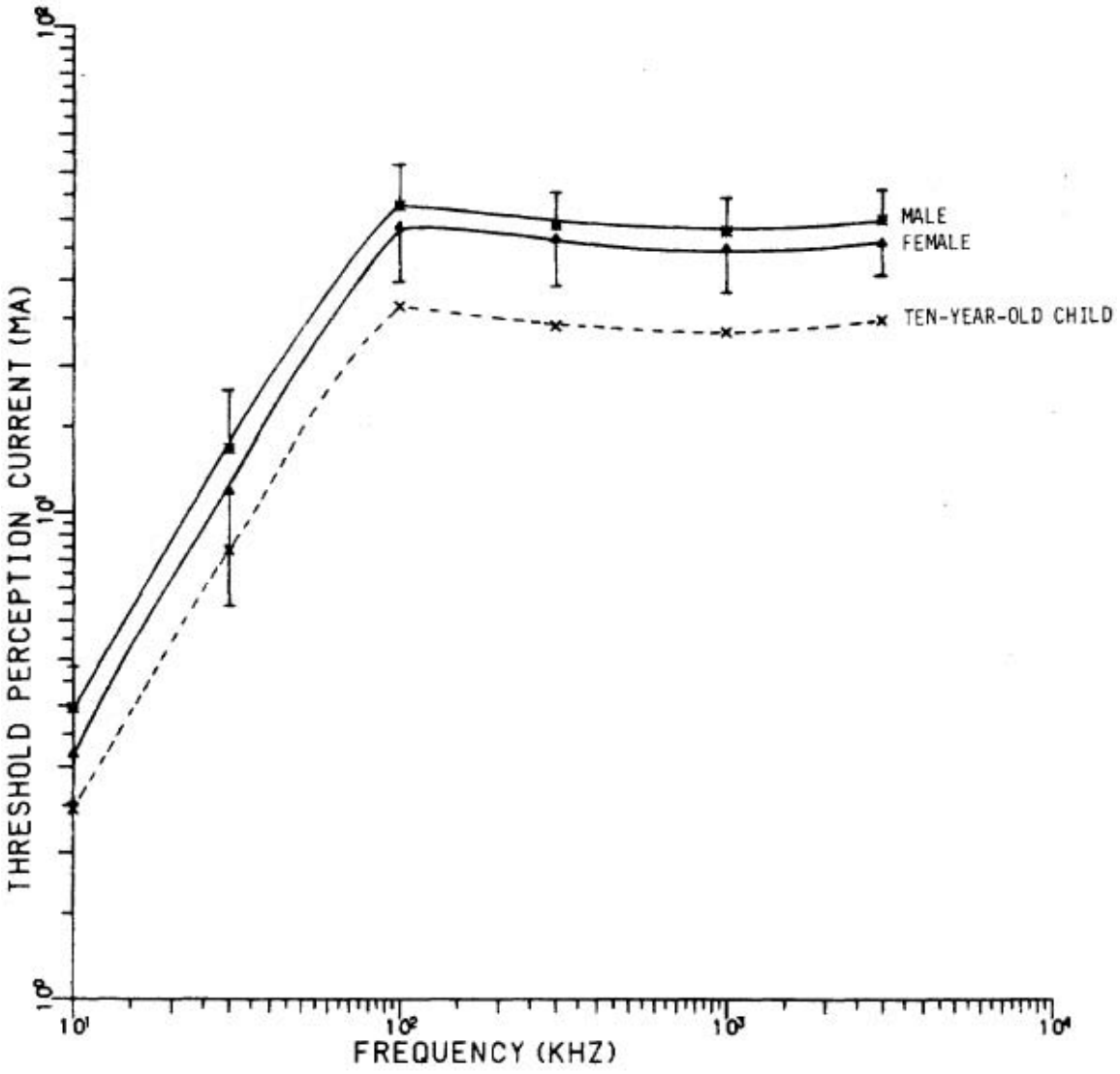

Figure 2-7
Average threshold current for perception, finger contact (25 mm^2), for adult males (N=197), adult females (N=170) and ten year-old children. Reproduced with permission from Chatterjee et al. (1986). © IEEE 1986.

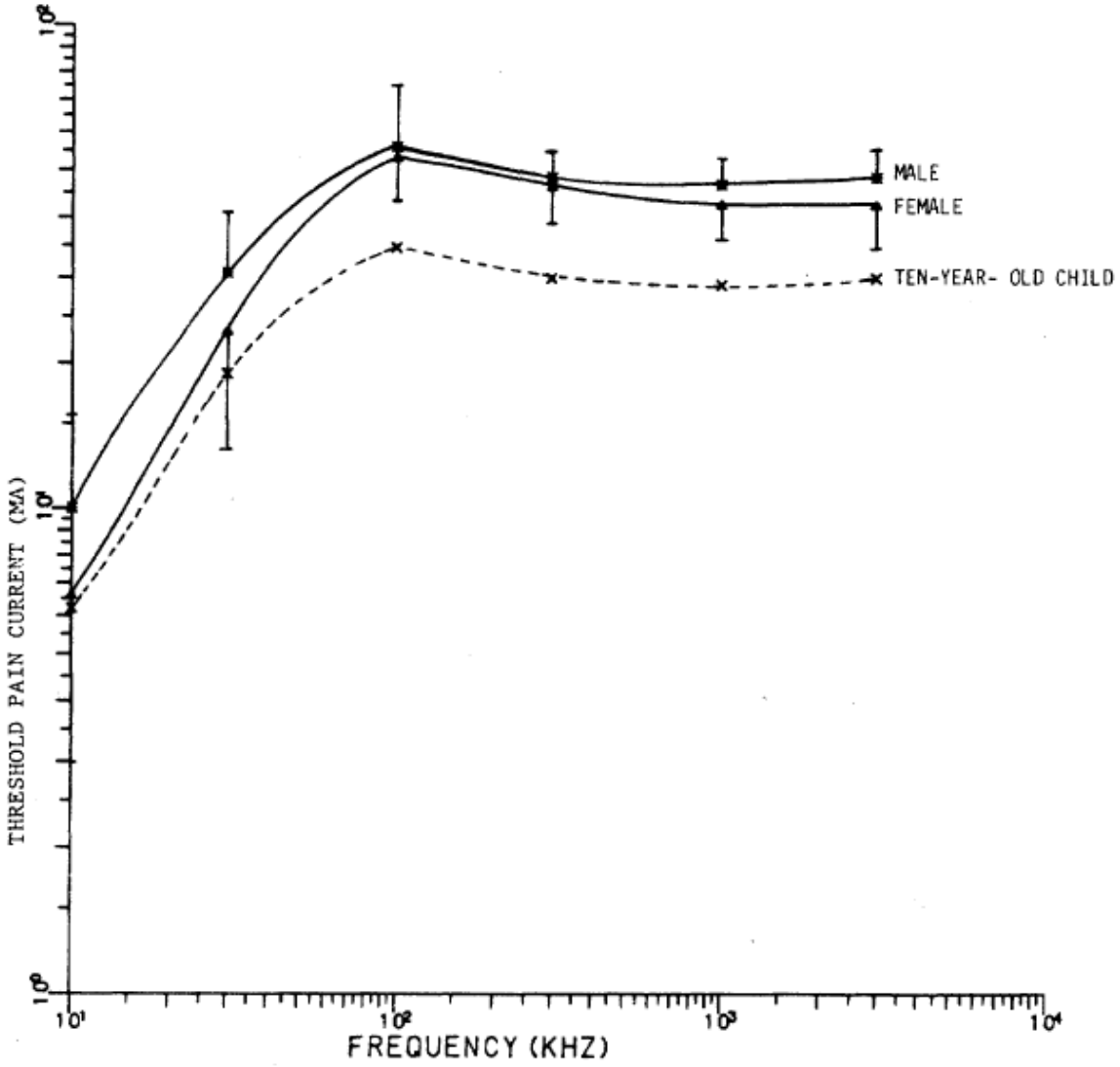

Figure 2-8
Average threshold current for pain, finger contact (25 mm^2), for adult males (N=197), adult females (N=170) and ten year-old children. Reproduced with permission from Chatterjee et al. (1986). © IEEE 1986.

In the quest for a meaningful predictor of potential RF burn hazards, the U. S. Navy conducted tests in the early 1970s that has formed the basis for the most used criteria for assessing possible hazards (Navy, 1982). Based on earlier work (Navy, 1973), it was concluded that when open circuit voltages of more than 140 volts rms existed on conductive objects, personnel contacting the object were likely to experience sparking between the object and the point of contact with a subsequent RF burn. Since that time, the 140 volt criteria has been used in many cases as the determining factor of whether workers would be subject to an RF burn when contacting an energized object. The open circuit voltage value is found in the latest revision of the IEEE Standard C95.1.

Today, it remains a question as to whether the 140 volts criterion is an accurate measure of RF burn hazards and, if so, does it pertain to any RF burn other than those experienced via electrical arcing to the surface of the skin (For example, how well does it apply to direct contact between the skin and the energized conductor?). The question arises as to what happens when an electrical arc penetrates the skin surface. While the skin is a relatively nonconductive tissue when compared with muscle tissue, the impedance to an RF current presented by the deeper lying muscle tissue would be substantially less. What are the implications of these spatial changes in tissue impedance to RF arc phenomena?

Technical Approach to Study

An investigation of minimum open circuit voltages sufficient to initiate an electrical arc at radio frequencies was deemed of high priority in this study with an emphasis on generating voltages of at least 140 volts rms. Hence, apparatus was designed that would permit evaluating the voltage that would be required for an arc to occur between two electrodes. The circuit used for this part of the experimentation evolved over a period of time but the final design that was used is illustrated in Figure 2-9.

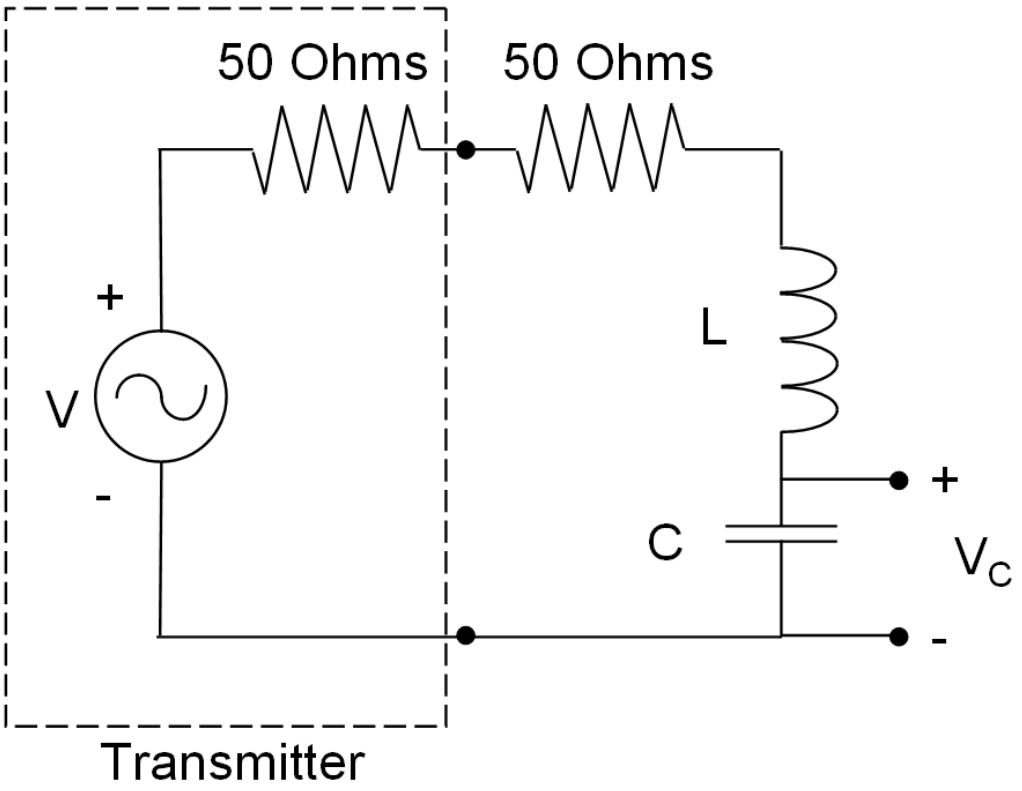

Figure 2-9
Circuit diagram of the apparatus used for generating high RF voltages for use in the experiment to create RF burns.

The circuit consists of a source of RF power in the form of an amateur radio HF transceiver (Elecraft model K3) with a 50 Ω output impedance capable of generating 120 watts of RF output power within selected amateur frequency bands from 1.8 MHz to 54 MHz. The output of the transceiver was connected to a series circuit composed of an R = 50 ohm, 100 watt, non-inductive dummy load resistor (Ohmite model LN100J50R), an air core inductor (MFJ Enterprises model 404-0669) (2" in diameter and 12 " long with 100 turns of number 12 wire) having a calculated low frequency inductance of L = 74 microhenries (μH) and a variable capacitor (MFJ Enterprises model 282-2008-1) having a maximum capacitance of C = 250 picofarads (pF). Subsequent evaluation of the inductor at 1.9 MHz with an antenna analyzer (AEA Technologies model CIA-HF) indicated that the reactance was 498 ohms. The object of the circuit was to create a resonant circuit that would have a sufficiently high RF voltage across either the capacitor (i.e., VC in Fig 9) so that an arc gap could be placed across the capacitor to result in an electrical arc across the gap. Initially, the goal for this voltage was to obtain at least 140 volts rms since this is the value the US Navy reports as the threshold for RF burns.

By varying the output power (P) from the transceiver, the voltage across the capacitor and the inductor would vary in accordance with the respective capacitive and inductive reactance within the circuit and the current. Since in a series resonant circuit the capacitive and inductive reactances cancel one another, the current is determined by the load resistor and power delivered to the load resistor as shown in Equation 2.

$$I = \sqrt{\frac{P}{R}} \qquad \textbf{(Equation 2)}$$

In the circuit of Figure 2-9, the current flowing at resonance at several different frequencies and power levels is listed in Table 2-1. The corresponding voltage across the capacitor can be found using Equation 2.

$$V_C = -j\frac{I}{2\pi fC} \qquad \textbf{(Equation 3)}$$

Table 2-1
Current at Resonance for Circuit in Figure 2-1 at Selected Frequencies for Different Power Levels with an Assumed Inductance of 42 μH and Capacitance of 168 pF

Frequency (MHz)	Power (W)	Current (mA rms)	Voltage (V_c rms)
1.9	1	141	70.2
1.9	10	447	223
1.9	100	1414	704
3.9	1	141	145
3.9	10	447	460
3.9	100	1414	1455
7.2	1	141	268
7.2	10	447	849
7.2	100	1414	2687

Table 2-1 shows that with the apparatus as defined, voltages across the capacitor or inductor could conceptually reach values nearly as great as 2700 volts. Hence, the circuit can be used to generate voltages well in excess of 140 volts rms.

As noted earlier, the intent of the project was to generate RF arcs between two electrodes connected across the capacitor as illustrated in Figure 2-10. In this figure, the circuit is represented as a Thevenin equivalent. For this equivalent circuit, the open circuit voltage is that shown in Table 2-1 and the Thevenin impedance can be determined from the circuit shown in Figure 2-11. Before moving on to experiments, it is necessary to also understand the amount of current available to the arc. This can be determined from an examination of Figure 2-10. For operation at 1.9 MHz, the minimum current is at least approximately 28 mA and the maximum about 278 mA. If the threshold for an RF burn were 50 mA, then the minimum RF voltage needed is approximately 126 volts.

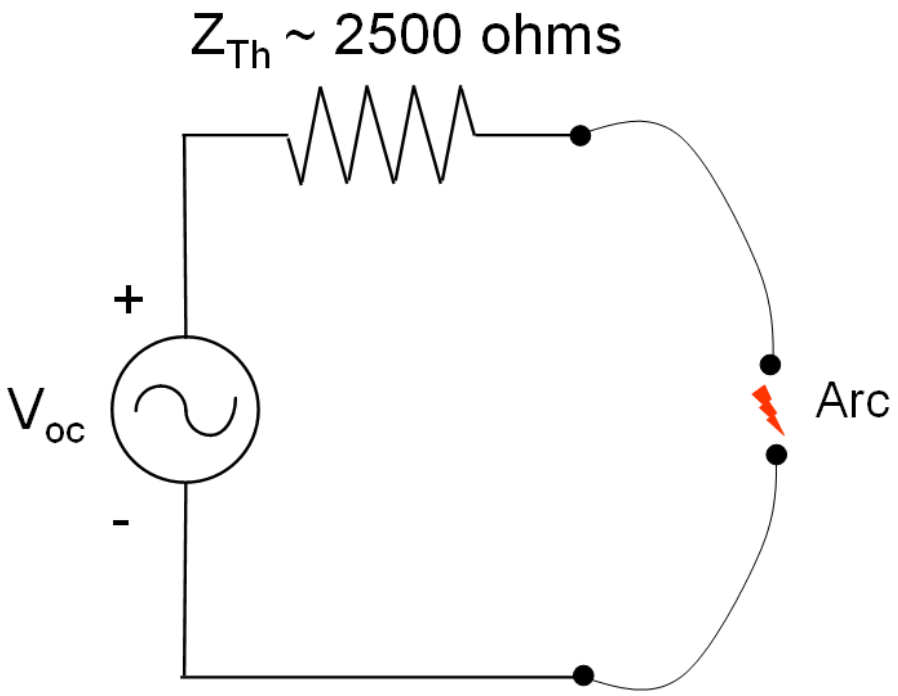

Figure 2-10
Thevenin equivalent circuit of apparatus for driving an arc.

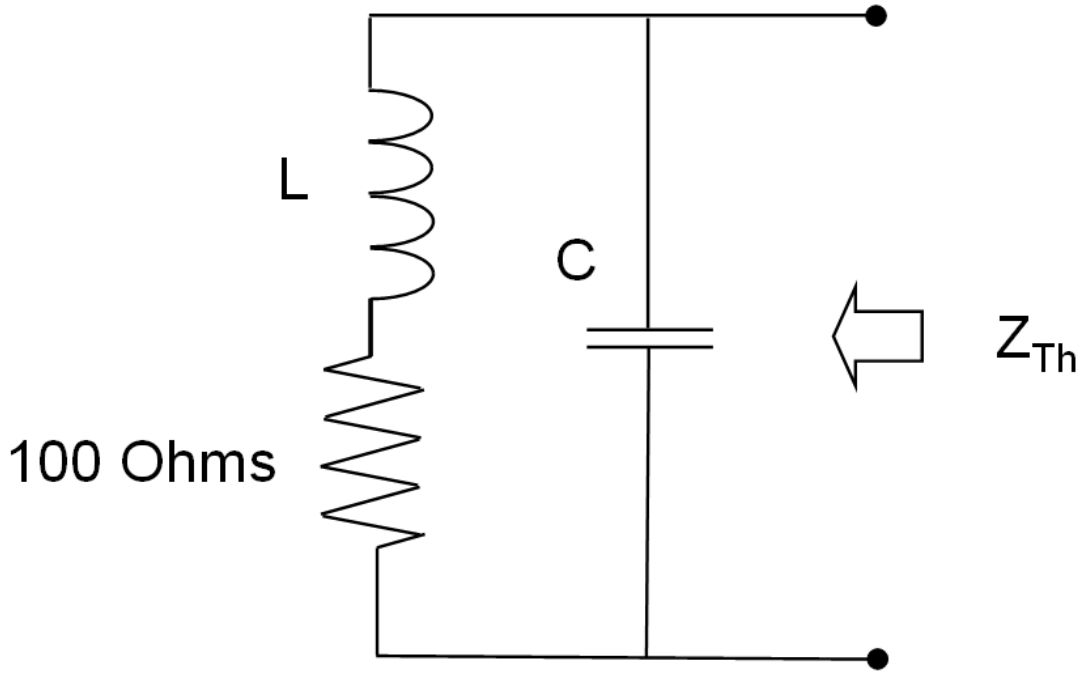

Figure 2-11
Circuit for evaluating the Thevenin impedance (i.e., V set to zero in Figure 2-9).

Again, one purpose of this work is to study the effect of RF arcs separately from the heating effect of RF contact currents. The first step in this process is to determine the minimum voltage needed to create an obvious arc. This is done using the circuit shown in Figure 2-9. For these experiments, the voltage V_C is increased until an arc is visible prior to contact.

A photograph of the actual apparatus as used in the work is shown in Figure 2-12. All of the work reported here was conducted at a frequency of 1.9 MHz. Two RF current transformers were used to monitor the current flowing in the complete circuit and in the electrode burn wire lead. An Ailtech model 94111-1 transformer was used with a Fluke model 8060A True RMS Multimeter to monitor the current flowing in the complete circuit and a Stoddart Aircraft Radio Company model 91550-1 transformer was used in conjunction with a Fluke model 87 True RMS Multimeter to measure the current flowing in the electrode burn wire (14 gage copper having a diameter of 1.628 mm). Calibration curves of the transfer impedance for the two current transformers were used to convert the voltage readings obtained with Fluke model 85RF probes. Each current transformer was terminated with a 50 ohm termination prior to connection of the digital multimeters.

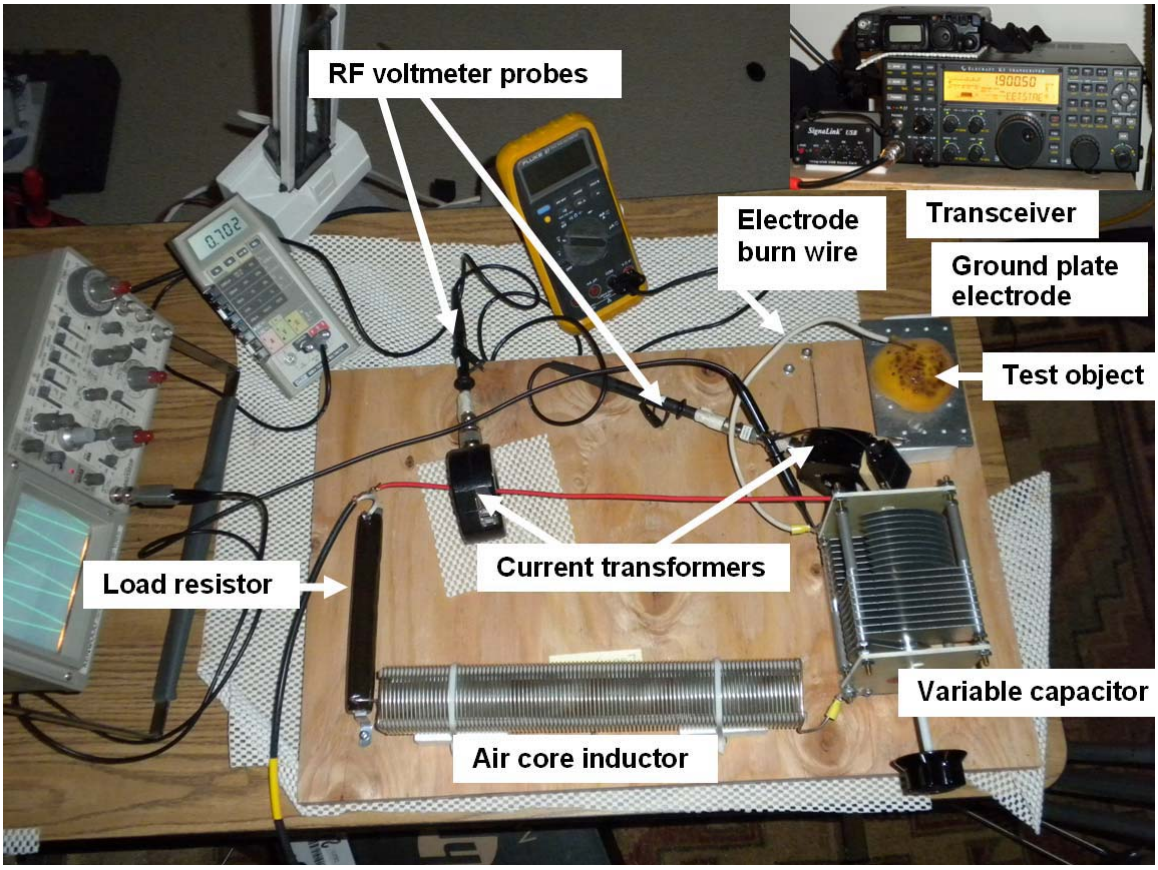

Figure 2-12
Photograph of the experimental apparatus used to study RF burns. The transceiver used to the drive the circuit is shown in the upper right inset.

A Kenwood model CS-1065 60 MHz oscilloscope with a model PC-29 probe having an input capacitance of less than 18 pF was connected across the capacitor terminals to obtain a voltage reading that could be related to the main circuit current flow readings. The oscilloscope had a maximum measurement capability of 400 volts peak-to-peak (equivalent to 141.4 volts rms) and, hence, was not used for routine use of the apparatus. While initial calculations indicated that an open circuit voltage on the capacitor might be approximately 700 V, a maximum value of 453 V was obtained in practice.

Preliminary Results from Arc Tests

The test apparatus was used to produce open circuit voltage across the capacitor (V_{OC}) that might result in arcing between the electrode wire and the ground plate electrode. Initially, the oscilloscope was used to measure V_{OC} at the maximum voltage that the scope could handle. This value, expressed as an rms voltage was used with the measured current in the circuit to obtain a correction factor that would allow converting any measurement of current to a value of V_{OC}. Subsequently, a series of V_{OC} values was established by varying the power output of the transceiver and observing for visual and audible signs of arcing. It was noted that during the V_{OC} calibration process that the circuit had to be retuned for resonance when the oscilloscope probe was clipped to the capacitor vs. when it was disconnected. The presumption was made that V_{OC} remained essentially unchanged between the two conditions as long as resonance was maintained since circuit current remained approximately constant. Resonance was achieved by tuning the variable capacitor for minimum reflected power as indicated by a meter on the transceiver.

Table 2-2 summarizes preliminary data obtained from the apparatus for producing electrical arcs. Arcing was initiated by bringing the burn electrode wire to the surface of the ground plate electrode and attempting to draw an arc from intermittent contact. Small sparks would be readily observed in many cases.

Table 2-2
Summary of Preliminary Data on RF Arcing at 1.9 MHz

$I_{(CIRCUIT)}$ (mA)	V_{oc} (V_{rms})	$I_{burn\ electrode}$ (mA)	Notes on observation of arcing
146	56.1	17.7	No indication of arcing
185	71.4	24.3	Barely detectable
222	85.6	31.5	Barely detectable
294	113	43.2	Clearly visible
368	140	46.4	Clearly visible
443	171	69.9	Very obvious
520	201	83.9	Very obvious
587	226	84.1	Very obvious
664	256	83.9	Very obvious
735	453	83.9	Very obvious

Table 2-2 data indicate that under the test conditions used, electrical arcing could be visually observed with V_{OC} of 71.4 V or more. Two important notes are relevant. Even with lower V_{OC} values, while no arc could be seen or heard, physically touching the wire electrode with the index finger elicited an immediate thermal pain response and withdrawal from the wire. The implication of this finding is that pain reactions can occur without the presence of electrical arcing. Secondly, the unchanging burn electrode current above a circuit current of approximately 520 mA is likely a result of the automatic power reduction provided by the transceiver in reaction to the mismatch caused by shorting the capacitor. Each time that the burn electrode wire was touched to the ground electrode plate to obtain a steady measure of the short circuit current ($I_{BURN\ ELECTRODE}$), the resonance of the circuit was altered, resulting in a mismatch to the transceiver. In order to protect the transceiver output circuit, it reduces its output power. Hence, while setting up the V_{OC} condition, the circuit is resonated but when the burn electrode is shorted to ground, if the output is already at an elevated power level, the transceiver reduces its power.

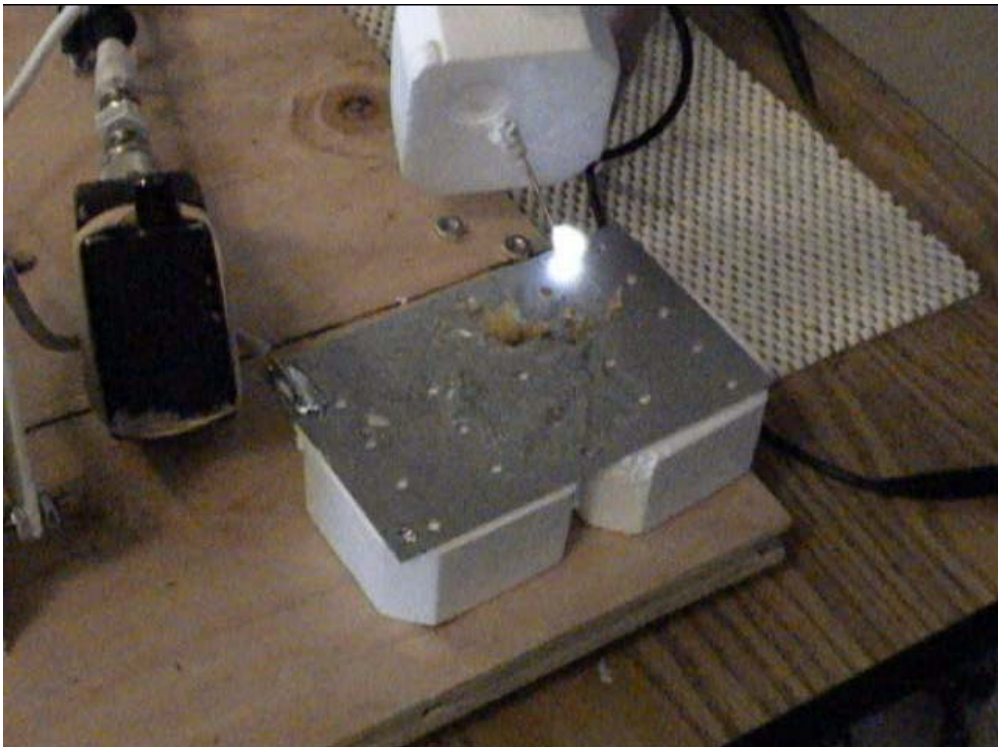

Figure 2-13
Arc between the burn wire electrode and the ground plate electrode at the maximum V_{oc} (453 V rms) achievable with the test apparatus.

Figure 2-13 shows one of the arcs obtained with the maximum V_{OC} possible (453 V rms) with the test apparatus. In this photo, the Styrofoam insulator around the burn electrode wire can been seen. Once an arc had been "struck" by momentarily lightly touching the ground plate, the arc could be drawn out to approximately one-half inch in length before it would extinguish. This

example is far more impressive than the arcs produced at lower voltages, including the 140 V value used as an RF burn criterion by the U. S. Navy.

A measurement of the apparent impedance presented by the variable capacitor was accomplished by using the oscilloscope to make measurements of V_{OC} with and without the burn electrode wire inserted into the load represented by the peach. At the same time, the current flowing into the load was measured. For example, with the load connected (burn electrode wire inserted into the peach), V_{OC} was observed to reduce from 140 V to 46.7 V while the load current was 44.9 mA. These data indicate that the impedance of the capacitor as a voltage source was approximately 2078 ohms. This is in the range of the value obtained from the Thevenin equivalent circuit analysis (2529 ohms)

The next experiment was to determine the damage that such an arc can do to an object that simulates the human system as much as possible. According to research dermatologists, the ideal model is that of recently slaughtered pig skin. An experiment designed to use this is shown in Figure 2-14 represented by one-half of a peach with the cut side in contact with the ground electrode plate.

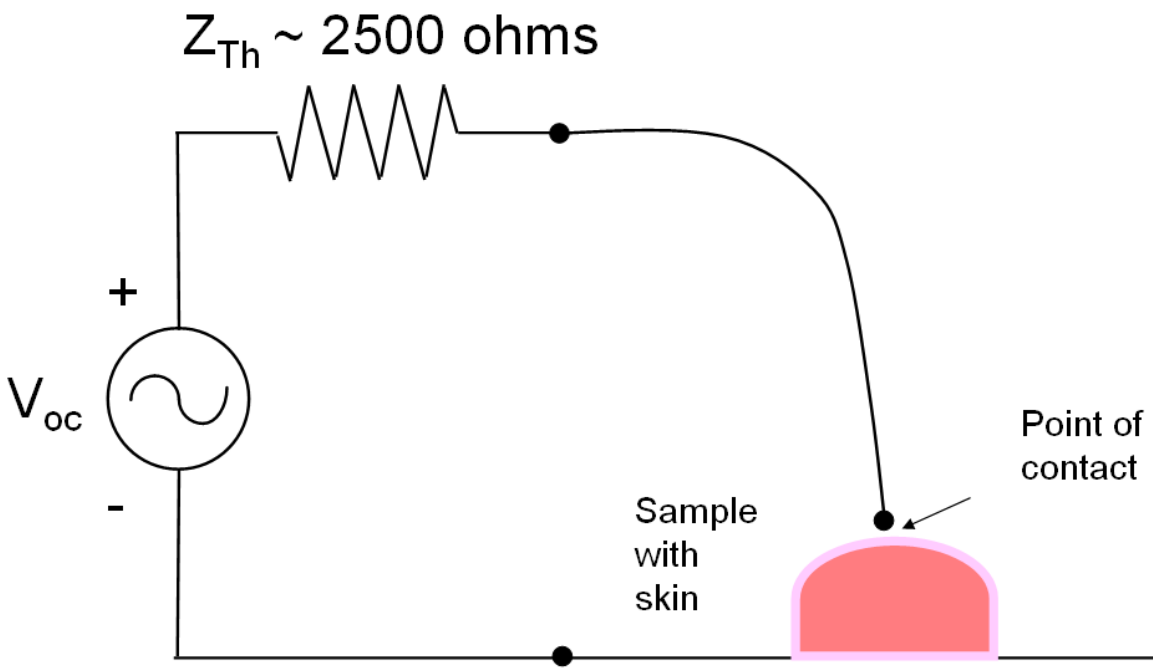

Figure 2-14
Apparatus for determining the RF burn damage to skin.

To investigate possible RF burn damage to skin, a surrogate for actual human skin was necessary despite the fact that one of the authors sustained a number of small point accidental burns during the course of these experiments. While human skin surrogates have been prepared by various researchers to study burns, a more accessible option was to use a peach. The peach presents a wet fleshy interior covered by a relatively dry and thin skin. These properties somewhat mimic

the case for human skin. For experimental purposes, a fresh peach was cut in half such that the flat cut side could be placed directly onto the surface of the ground electrode plate. To look for RF burning, the burn electrode wire was manually brought to the surface of the peach skin and moved in a small circle with the tip of the wire just barely touching the peach's skin. At higher V_{OC} values, relatively large arcs could be produced, almost similar to arc welding. Rather than the arc existing between the burn electrode wire and the ground plate, the arc was produced at the surface of the peach. Figure 2-15 illustrates an example of what the arcing can look like at higher V_{OC} values. The initial experiments have shown that when using a peach (that has a very thin skin) it is possible to induce visible damage due to arcing. This is evident in Figure 2-15 where the obvious bright arc appears as well as numerous other burn marks from experimentation. In this figure, the burn electrode wire is shown being positioned by direct contact with the hand of the operator. For all measurements in which quantitative data were obtained, such as load currents, the wire was positioned with use of a Styrofoam block that isolated the hand from the wire sufficiently such that there was no change in the matching condition imposed on the transceiver due to capacitive coupling between the hand and the circuit.

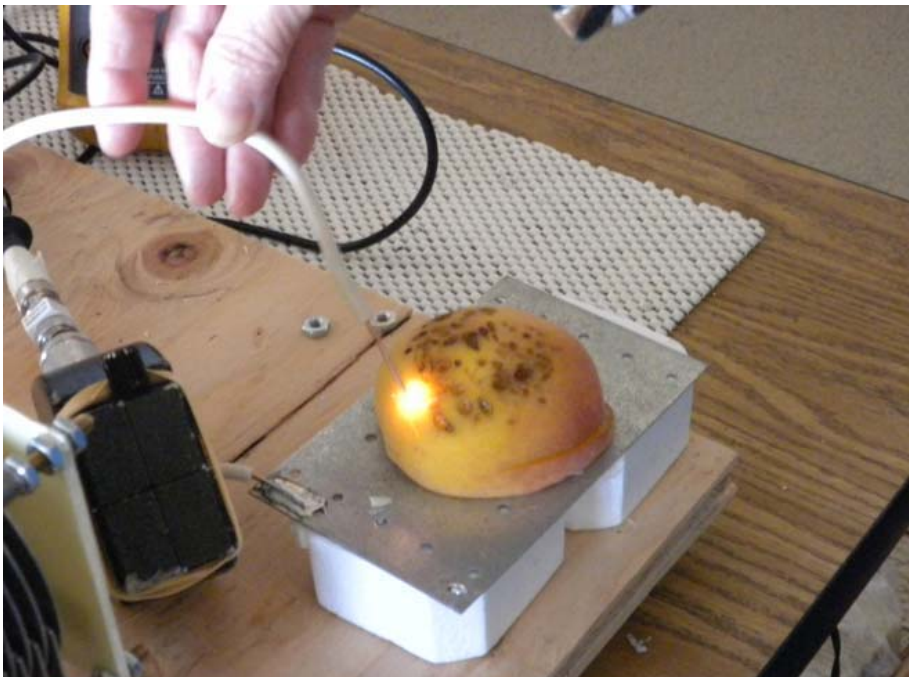

Figure 2-15
A test peach as a human skin surrogate for evaluating the possibility of RF burns. The bright spot is the point on the peach where the electrical arc contacts the surface.

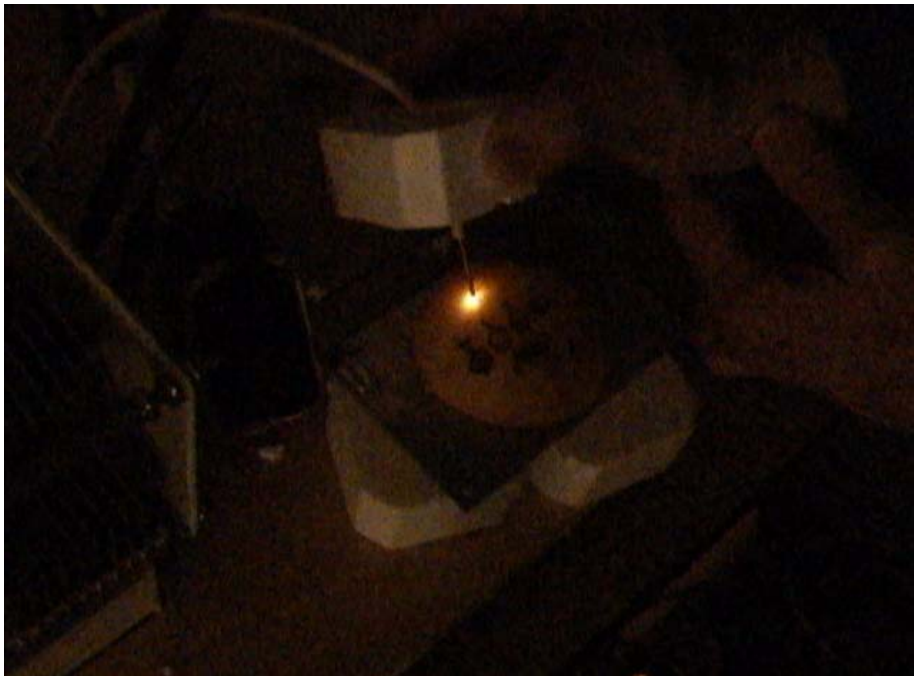

Figure 2-16
Arc between the burn wire electrode and the peach at V_{oc} (140 V rms). Photograph taken in darkness to enhance visual aspect of the arc.

Although not as dramatic as the higher voltage arcs, even at V_{OC} of 140 V rms, highly visible arcing can be seen as shown in Figure 2-16. This photograph is one frame from a movie made of the arcing process while the burn electrode wire was placed lightly against the skin of the peach and "dragged" about the surface.

Finally, Figure 2-17 provides a rough gradation of visible RF burn damage where four different V_{OC} values with associated load currents were used to produce burn marks on the peach skin.

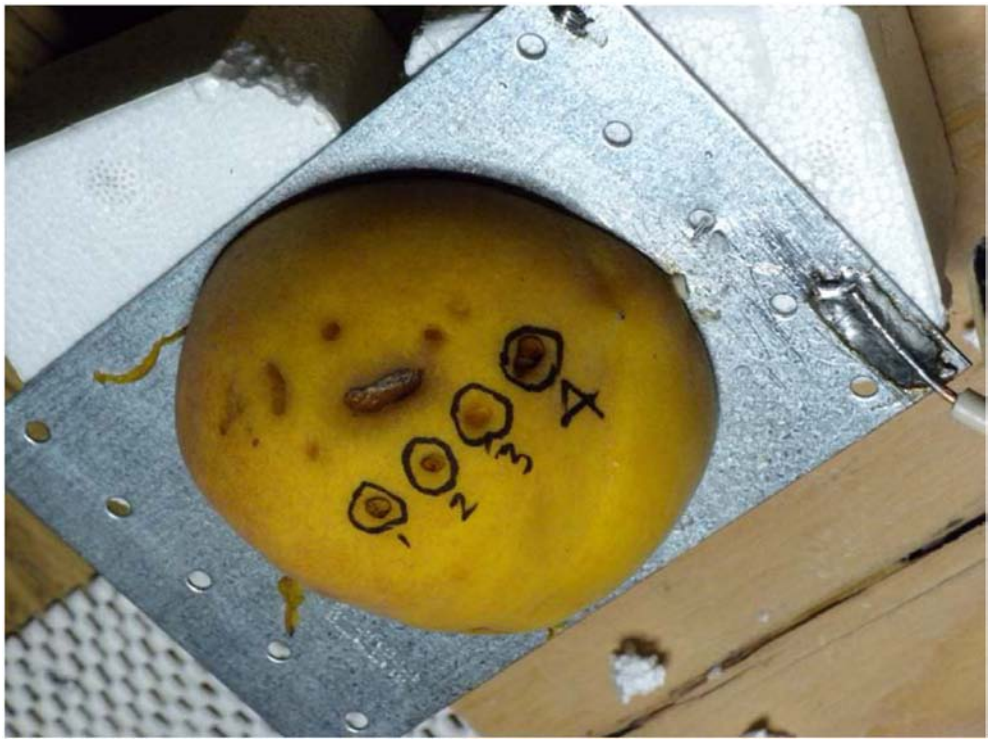

Figure 2-17
Series of RF burn marks made with different V_{oc} values and load currents. (1) 140 V, 46 mA; (2) 85.6 V, 31.5 mA; (3) 56.1 V, 17.7 mA; (4) 171 V, 70 mA).

The qualitative nature of Figure 2-17 helps to illustrate the difficulty in quantifying the parameters relevant to RF burns. Tissue burning is a function of current density and time. So, one may achieve the same level of thermal damage from an RF burn at a lower open circuit voltage and/or load current as when using higher voltages and currents. The exposure time makes the difference. At some point, however, and this is difficult to quantify with any precision, the local current density becomes sufficiently low as to not result in burning regardless of the exposure duration. Target 3 in Figure 2-17 represents a very low current of approximately 18 mA and shows less thermal damage than the other higher voltage and higher current burn sites. Nonetheless, damage can occur if the conditions are such that the point of contact can exist for enough time to allow the tissue to become hot assuming that the current density is sufficient to cause heating.

Insights Gained

An RF burn represents a complex phenomenon despite the fact that it is simply a thermal interaction with body tissue. RF burns depend on the flow of current through very limited regions of tissue, i.e., current density. Sufficient voltage, however, must exist to drive this current and the impedance presented by the tissue affects the magnitude of current that will flow. Further, whether a burn is produced may, in some cases of direct contact with energized conductors, depend on the duration of the exposure (how long a given current density exists).

Actual tissue damage is apparently determined by the product of temperature that the skin, or underlying tissue, reaches during exposure to a given current density and duration of exposure. Since heating will be determined by the local energy delivery rate, i.e., the product of current density and time (energy density), energy density will be a direct factor in determining the potential RF burn hazard.

The qualitative results of experiments reported here are consistent with research associated with electosurgery (a general term that includes the use of RF energy for cutting and coagulating in surgical operations). For example, tissue cutting typically involves the use of fine gage wire electrodes, including needle type tips, with high RF voltages. Electrosurgical units (ESUs) are RF generating devices that are used for surgery. These devices work on the principle of delivering highly localized RF energy at a sufficiently high rate to the tissue to effectively desiccate the tissue (evaporate the water content), resulting in a burn or cut through the tissue. Figure 2-18, taken from a manual for teaching physicians the techniques of electrosurgery, shows how higher voltages cause surface burning at the interface of the "cutting electrode" with the tissue. This is normally caused by the production of electrical arcs from the electrode to the tissue. A small shower of sparks that terminate on the tissue surface result in extremely high current density at the point of contact of each of the sparks. These very high current density points result in surface burning, charring, or, in medical terminology, fulgarating. Figure 2-18 illustrates a progressively thicker charring effect on the sides of the RF incision caused by raising the electrode voltage to a high enough value.

Absten (2002) states that tissue cutting requires an electrode voltage of at least 200 peak volts (this is equivalent to 141 V rms. Hence, the 140 V criterion recommended by the Navy would appear to be at the lower threshold for electrosurgical use. In the medical application however, the electrodes must be kept consistently on or very near the tissue being incised.

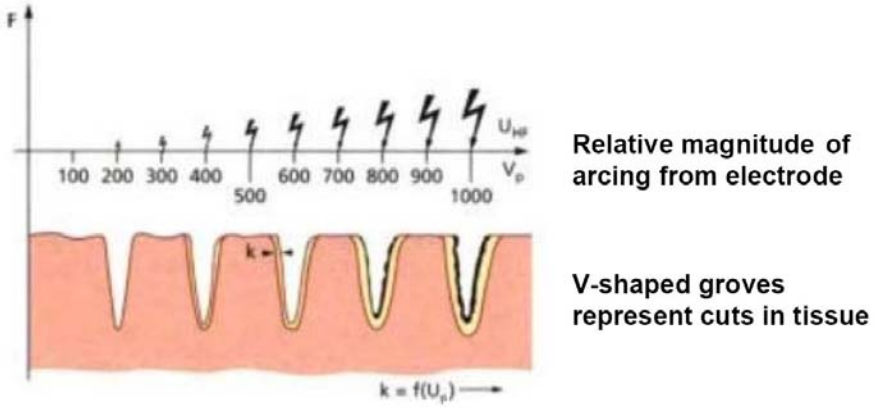

Figure 2-18
Tissue effects as affected by voltage and resistance. Reproduced with permission from Gregory T. Absten, Professional Medical Education Association, Inc., www.LaserTraining.org. Adapted from Absten, G. T. (2002). [*Practical Electrosurgery for Clinicians*, Figure B1.]

A potentially useful report in the medical instrumentation literature offers strong support for the hypothesis that local energy density is the best correlate to skin damage from RF burns (Pearce et al., 1983). Pearce and coworkers describe experiments with pig skin using an ESU operating at 500 kHz and determined current density at the application electrode and time to produce burns of varying degrees. They used a parameter that they called the "relative energy density factor" defined as the product of the square of current density (amperes per square centimeter) at the electrode and time (seconds) as the most accurate indicator of thermal damage to the skin. Using 34 skin sites on anesthetized pigs, graded levels of "average electrosurgical current density" were delivered for specified times. The severity of cutaneous response was determined by gross and microscopic study 56 hours later. Results from their report have been graphically illustrated in Figure 2-19.

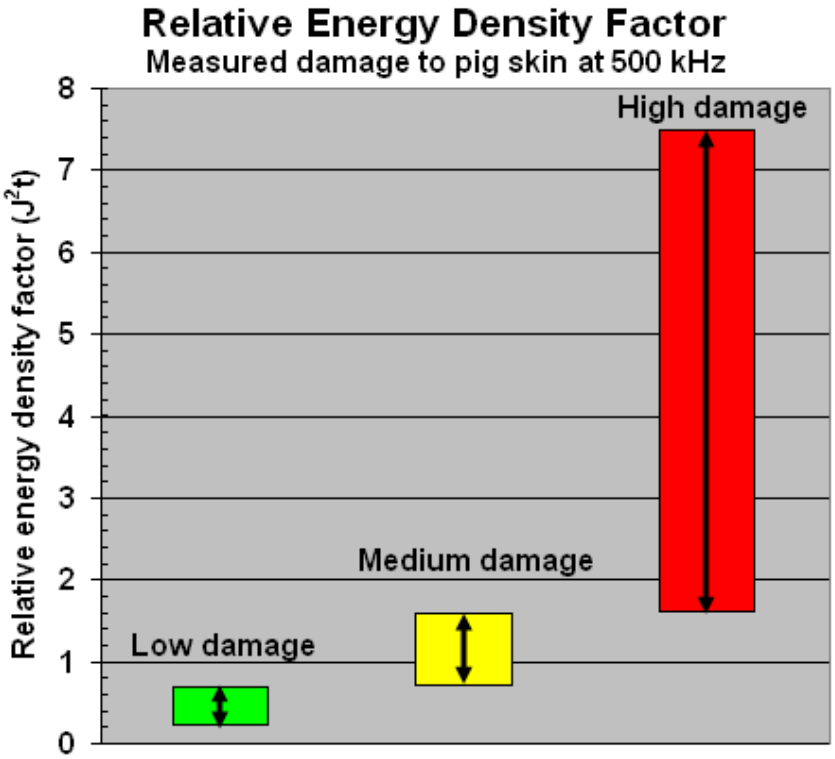

Figure 2-19
Relative energy density factor for pig skin subject to 500 kHz electrosurgical currents for low, medium and high degrees of thermal damage to the skin. Graphical presentation of data from Pearce et al. (1983).

Pearce et al. categorized the observed effects into low, medium and high degrees of thermal skin damage according to their relative energy density factor with values corresponding to 0.2 to 0.7 J^2t, 0.7 to 1.6 J^2t and 1.6 to 7.5 J^2t respectively. They reported that at nine of 10 skin sites, the low range of energy density factors resulted in maximum skin temperatures in the range of 38-47 ºC with either no damage or mild second-degree burn lying just beyond the electrode contact zone. At the medium range of energy density factors at 9 of 11 skin sites, maximum skin temperatures in the range 49-55 ºC with single or multiple rings of second-degree burns located

just inside or beyond the rim of the electrode. At the maximum range of energy density factors, all 13 sites so exposed exhibited maximum temperatures of 55 to 81 ºC. These burn sites were the most severe and produced with white to brownish, dry, firm, third-degree burns surrounded by peripheral rings of second-degree burns. They noted that if skin temperatures were less than 45 ºC, no significant skin damage was produced corresponding to an energy density factor of 0.75 J^2t. Presumably, this value of energy density factor could be used as a threshold for actual damage. This does not mean that significant pain might not be produced.

Using the relative energy density factor described by Pearce et al. (1983), the RF current that would be required for a range of exposure durations from 0.1 second to 5 seconds and for a range of contact areas from 2.082 mm^2 to 100 mm^2 (1 cm^2) were computed and presented graphically in Figures 2-20 to 2-24.

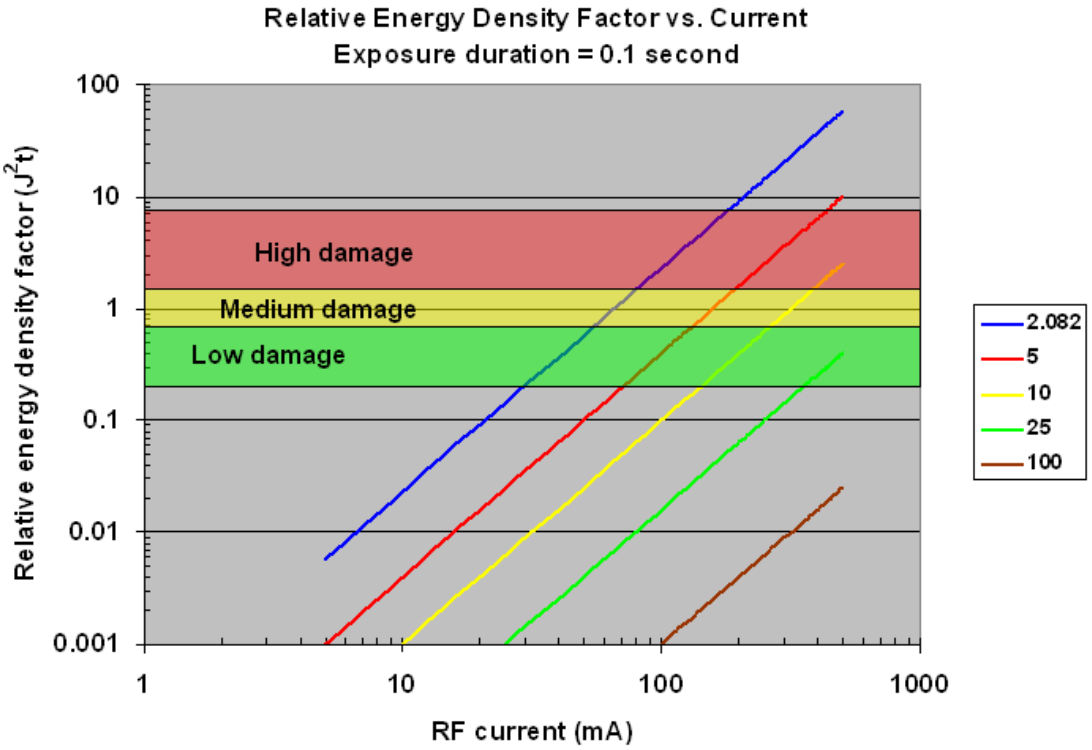

Figure 2-20
Relative energy density factor (after Pearce et al., 1983) for an exposure duration of 0.1 second and contact areas of 2.082, 5, 10, 25 and 100 mm^2.

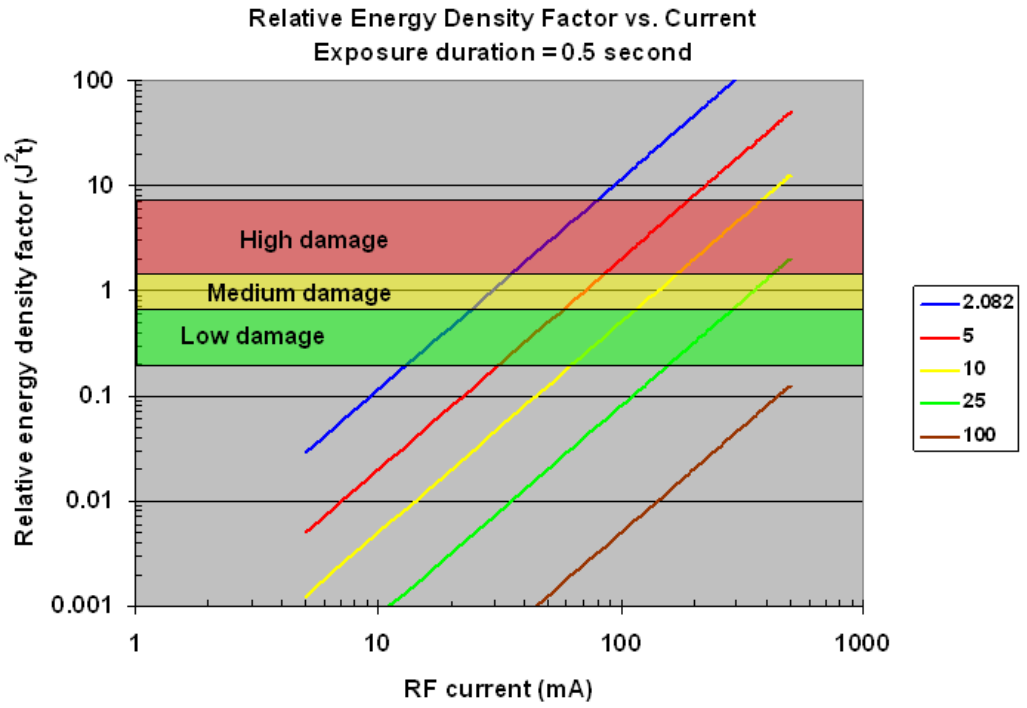

Figure 2-21
Relative energy density factor (after Pearce et al., 1983) for an exposure duration of 0.5 second and contact areas of 2.082, 5, 10, 25 and 100 mm^2.

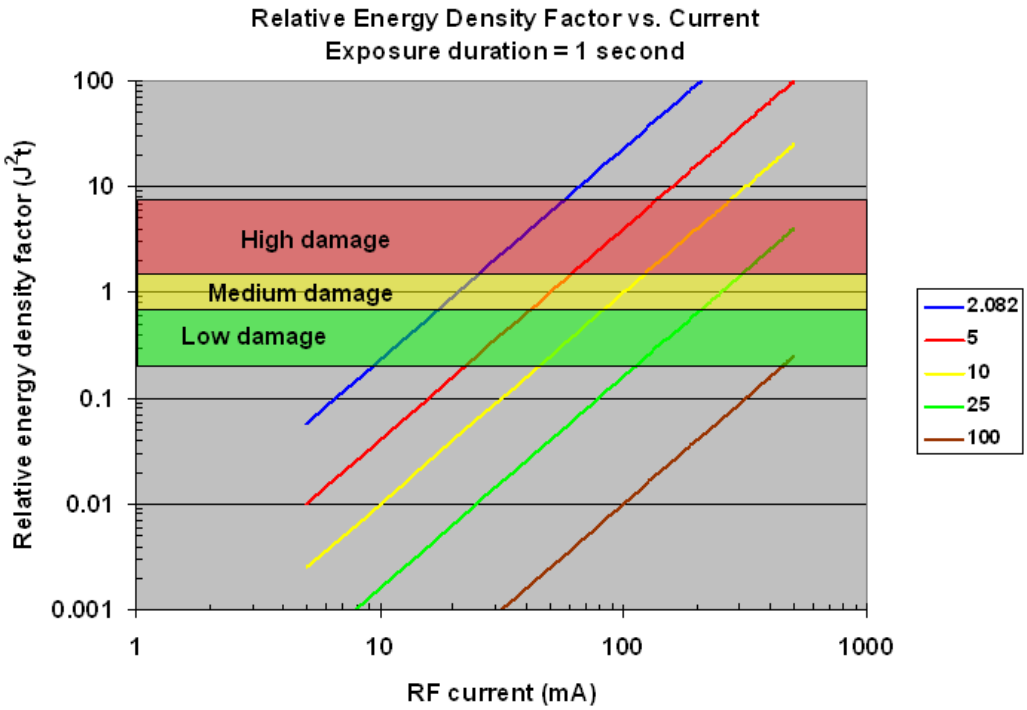

Figure 2-22
Relative energy density factor (after Pearce et al., 1983) for an exposure duration of 1 second and contact areas of 2.082, 5, 10, 25 and 100 mm^2.

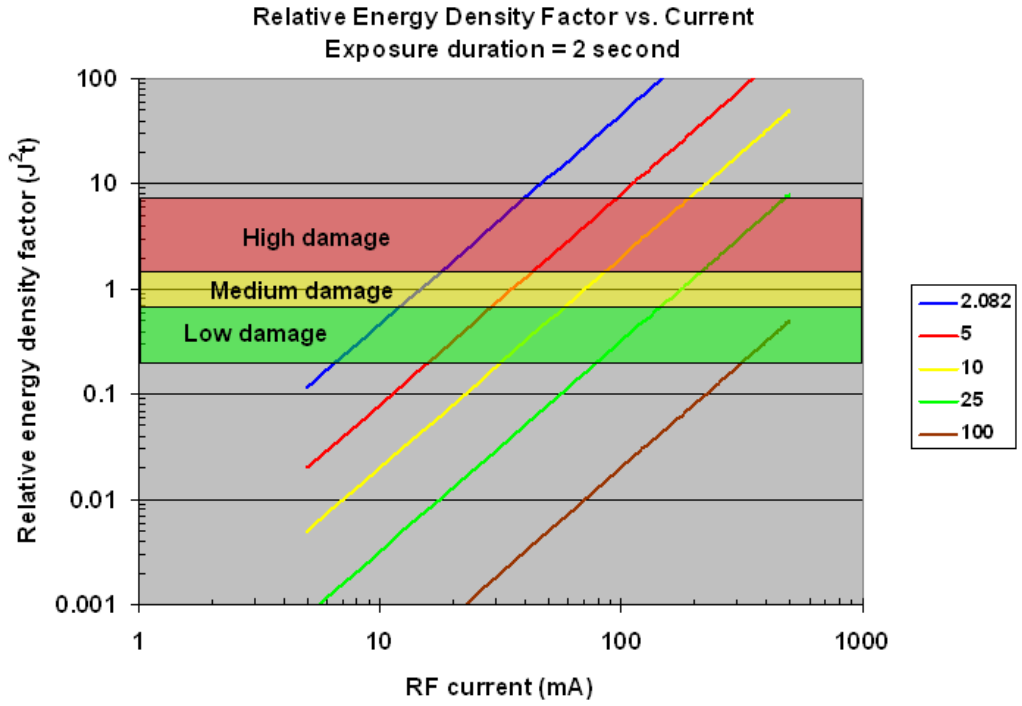

Figure 2-23
Relative energy density factor (after Pearce et al., 1983) for an exposure duration of 2 seconds and contact areas of 2.082, 5, 10, 25 and 100 mm^2.

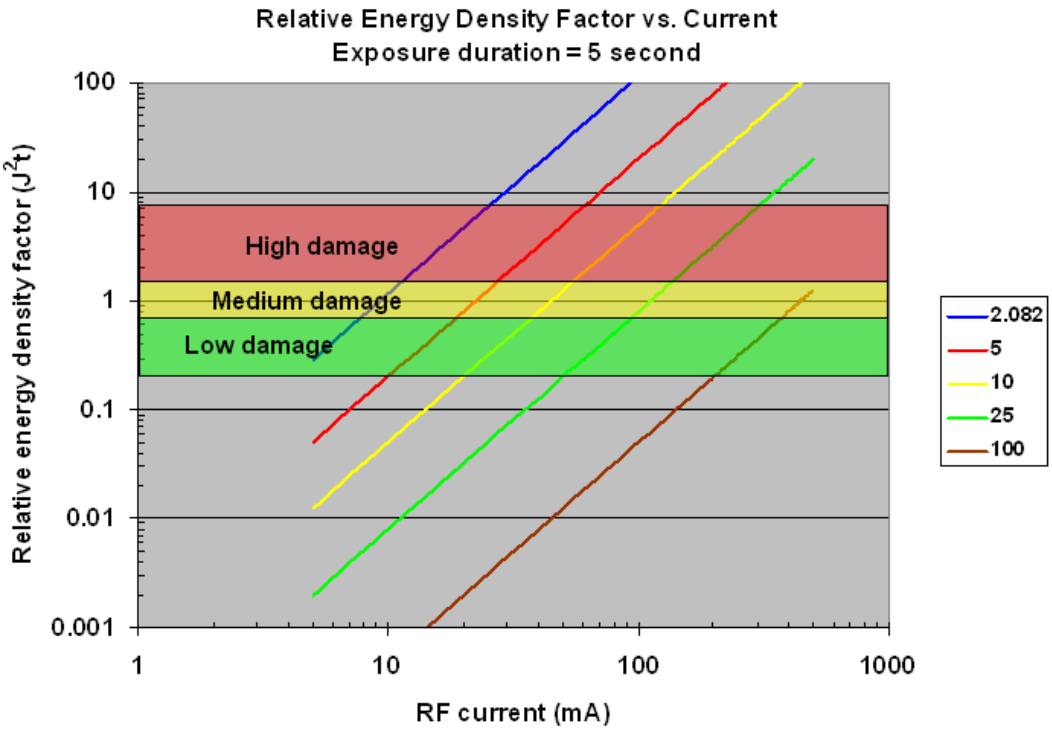

Figure 2-24
Relative energy density factor (after Pearce et al., 1983) for an exposure duration of 5 seconds and contact areas of 2.082, 5, 10, 25 and 100 mm^2.

The exposure durations were set to small values that could be commensurate with typical field working conditions. In most cases when arcing occurs, withdrawal from the energized object will be immediate, hence the selection of 0.1 second as the smallest example exposure duration. Contact areas were selected to represent a range of values that included 1 cm^2, as this is a common area referenced in various literature citations, and the cross section area of an AWG number 14 solid wire. This is the wire size used as the "burn wire electrode" in the previously described experiments conducted as part of this project.

Tissue heating rate is directly related to the local current density. For example, specific absorption rate (SAR) can be expressed in term of current density as follows:

$$SAR(W/kg) = \frac{J^2}{\sigma\rho} \qquad \textbf{(Equation 4)}$$

where
J is current density (A/m^2)
σ is tissue conductivity (S/m)
ρ is tissue mass density (kg/m^3)

The density of epidermis is 1200 kg/m^3 (Moon, 2006). Skin tissue conductivity was conservatively taken to be in the range of approximately 0.02 to 0.6 S/m in this analysis (because skin is dryer than the underlying tissues, its conductivity is less). A representative value of conductivity for muscle tissue is 0.6 S/m. The actual conductivity for skin may be considerably less, for example, in the range of 0.02 S/m. However, during the very fast burning process during an RF burn, the more conductive tissue just beneath the stratum corneum, the outer most layer of the epidermis, may more stongly influence the current flow.

Since SAR is a measure of energy absorption rate, it can be used to express an estimate of the rate of tissue temperature rise. From the basic heat equation:

$$Q = mc\Delta T \qquad \textbf{(Equation 5)}$$

where
Q is thermal energy (J)
m is the mass of tissue
c is the specific heat of the tissue (J/kg-ºC)
ΔT is the change in tissue temperature caused by the absorption of energy Q

Differentiating Equation 5 with respect to time results in the following expression:

$$\frac{dQ}{dt} = mc\frac{dT}{dt} \qquad \textbf{(Equation 6)}$$

Hence, with knowledge of how to express SAR from the current density and how to relate the time rate of energy delivery to the tissue to the increase in temperature, the time rate of temperature rise can be expressed as:

$$\frac{dT}{dt}(^\circ/\text{sec}) = \frac{SAR}{c} \qquad \textbf{(Equation 7)}$$

For instance, an SAR of 100 W/kg in a given mass of tissue will result in an expected temperature rise of about 0.03 ºC/sec. The specific heat of epidermis tissue at 25 ºC is 3600 J/kg-ºC (Moon, 2006).

Normal human skin temperature has been found to range from nominally 25-34 ºC. In a clinical study (Agarwal et al., 2007) of 50 healthy persons (29 females, 21 males; average age 32.8 years). The mean skin temperature was measured to be 31.6 ± 2.1 ºC. A calculation of estimated adiabatic temperature elevation (i.e., no inclusion of cooling effects of blood flow, convection, or radiation) was performed based on the current density that would exist for various areas of contact with an energized conductor. Extrapolating the curve for pain in Figure 2-6, a temperature of approximately 53 ºC is estimated to result in pain for a brief exposure of 0.1 seconds. This would imply that a skin temperature elevation of 54-31.6 ºC or 22.4 ºC would be required from local current flow to cause thermal pain. Using the same Figure, an estimated temperature of just less than 62 ºC may be associated with necrosis of the skin for an exposure of 1 second which implies a skin temperature elevation of 62-31.6 ºC or 30.4 ºC. Figure 2-25 is a plot of the theoretical temperature elevation (with the assumption that all electrically generated heat remains in the local tissue with no cooling mechanisms at play) for a 0.1 second exposure duration of the current.

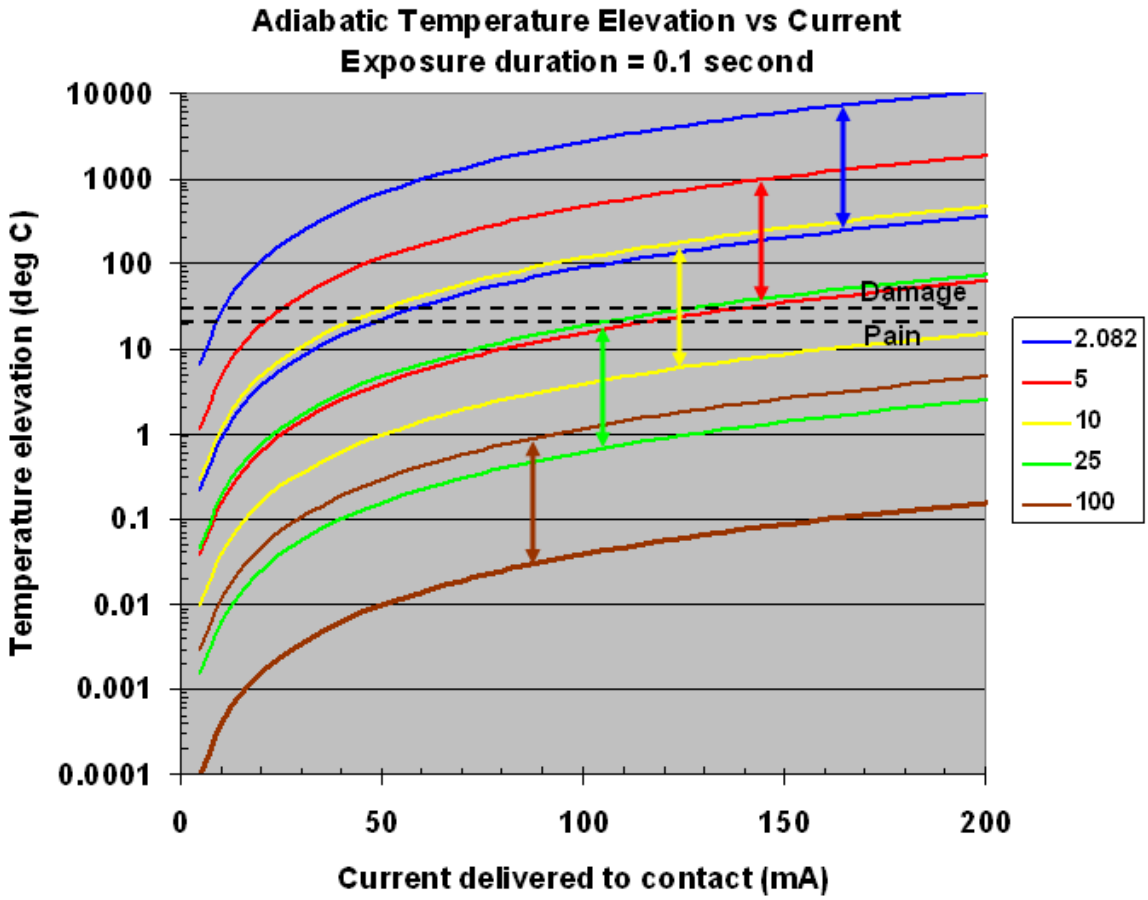

Figure 2-25
Theoretical temperature elevation vs. RF current for contact areas of 2.082, 5, 10, 25 and 100 mm^2 for current flow duration of 0.1 second.

SAR was computed for two different tissue conductivities, 0.02 S/m and 0.6 S/m, these representing the conductivities for skin and muscle tissue respectively. If during contact with a conductor, current flow is entirely through just the outer most layer of the epidermis, then the skin value is likely more appropriate. However, if arcing occurs, this could lead to penetration of the outer skin layer with the current within the arc reaching to the underlying tissue with a much high conductivity. Hence, two curves are presented for each contact area with the understanding that the true value lies somewhere between these two curves. Figure 2-25 indicates that a contact current in the range of about 10 to 50 mA could potentially cause a pain reaction in a 0.1 second exposure to the end of an AWG number 14 wire. Presumably, only a slightly greater range of currents could drive the temperature elevation sufficiently to result in a burn at the point of contact. Interestingly, the difference between the sensation of pain and tissue necrosis is related to only a modest difference in temperature elevation for the small contact area.

Conclusions

Two modes of creating RF burns can occur when handling energized conductors. Direct contact with the conductor will lead to current flowing between the conductor and the body of the individual touching the conductor. Joule heating, produced simply through the action of current and tissue impedance, results in elevating the temperature of the local tissue. If the rate of temperature elevation is great enough to overcome any heat dissipation that is inherent to the exposure situation, for example, circulatory system effects, heat conduction, and heat radiation, and if this delivery of energy to the local tissue happens within a very brief period, an RF burn may occur with little notice to the subject. An RF burn can, however, also occur via the mechanism of electrical arcing between the energized conductor and the person approaching the conductor. In this case, and depending on the voltage of the conductor, surface skin burning may happen with eventual direct physical contact between the skin and the energized conductor. Hence, RF burns may constitute a combination of different mechanisms that lead to almost instantaneous pain reaction if not actual tissue damage.

This review of the RF burn phenomenon has revealed that contact current limits specified in various standards for safe exposure to RF energy, for example 100 mA for occupational exposure, are not necessarily protective. If currents less than 100 mA occur during work, they may still lead to RF burns but this will depend on the surface area of contact between the individual and the energized conductor. These contact currents can be mitigated to a degree with insulated gloves (Tell, 1993) but the extent of electrical isolation provided by the glove can be frequency dependent with decreasing protection at higher frequencies where the capacitive reactance afforded by the glove is diminished. An alternative suggested in the literature involves the use of conductive gloves to enhance electrical connection to the energized object and spreading of the current to minimize current density and, thus, the likelihood of an RF burn. Clearly, though, 100 mA is not a conservative value for contact current if RF burns are to be avoided.

Further, the experimental data developed during this exercise indicate that the open circuit voltage criterion of 140 V used by the U. S. Navy (Navy, 1982) is not necessarily protective against RF burns. Open circuit voltages as low as 71 V were observed to cause minute sparks that if incident on the skin could lead to inadvertent and fast withdrawal from the situation. Such movements could result in accidental falls or other injuries. Open circuit voltages of 140 V were found to easily result in highly noticeable RF burns, the extent of burns being dependent on magnitude of arcing and duration of current flow. A tentative conclusion is that high RF voltage arcs without much current can still do damage.

In the experiments, it was observed that current flow through the surrogate target peach was essentially the same as the short circuit current to the ground plate electrode. There appeared to be little dependence on the length of the wire electrode in contact with the interior of the conductive interior of the peach. Once the wire had penetrated the skin of the peach, the current measured changed only very little with insertion depth.

The threshold for RF burns is related in a complicated way to local skin current density, i.e., area of contact and magnitude of current, as well as duration of exposure. This makes the task of characterizing a given RF environment difficult since an RF burn appears to not be solely a function of voltage or current alone but a combination. Skin temperature, while a determinate of whether actual skin damage occurs, is not practical to assess in field working conditions. Thus it is difficult to determine what the threshold for a burn is since it is so dependent on contact area and energy delivered to the tissue. And the fact that intermittent arcing between energized objects and the body can occur and may only be present for fleeting moments adds to the challenge of how best to characterize a given exposure situation relative to the risk of RF burns.

In many ways, RF burns are intimately related the practice of electrosurgery. The underlying basis of electrosurgery, in fact, uses RF energy applied in precise ways to burn through tissue. While medical practice focuses on the beneficial application of controlled RF burning, occupational health and safety programs must recognize the potential for RF burns in the work place and develop strategies to mitigate the hazard that is associated with them. However, there is much useful insight to the RF burn process that can be gained from the experiences of applying electrosurgical techniques in the medical literature.

Practically, workers need to understand that anytime they are close to active antennas or parasitic conductive elements in the environment of RF fields, caution should be used to avoid possible RF burns. In the context of the electrical power industry, for example, work to string transmission lines should include an assessment of whether there are any nearby AM radio broadcast stations prior to commencing with work. Ambient RF fields, particularly those produced by AM radio broadcast stations in the 0.535 to 1.710 MHz range, can couple significant energy from the station's electric and magnetic fields to long runs of cable. Depending on cable lengths, and especially if these lengths happen to be resonant with the frequency of the field, RF voltages can be developed on the cables that can easily exceed the threshold for electrical arcing to other points of different electrical potential. This phenomenon principally includes electromagnetic illumination of ungrounded structures wherein a grounded individual may approach the energized conductor, leading to an arc between the conductor and the person. Although not the focus of this report, mitigation of this type of hazard can in many instances be accomplished via grounding of the conductive structure that is exposed to the RF fields. Unfortunately, however, proper application of adequate RF grounding is not always obvious and in many cases may not be practical during common field work. For example, while the grounding of a large conductive loop composed of a power line shield wire across two or more support poles may eliminate the possibility of arcing to an individual who may contact a down lead from the wire, this same down lead could become a source of significant RF burn hazard if the ground connection is removed or accidentally broken. When the potential for RF burns exists at a work site, personnel should be made aware of precautions that should be followed to minimize the probability of incurring an RF burn.

3
RF BURNS AT VERY HIGH FREQUENCIES FROM CONTACT WITH PARASITICALLY ENERGIZED CONDUCTORS

Background

This chapter addresses the following question: Does compliance with maximum permissible exposure (MPE) levels ensure that radio-frequency (RF) burns will not occur when a person is in contact with a parasitically energized conductor? MPE levels were created to ensure that the fields induced in a human do not result in the limits on specific absorption rates (SAR) being exceeded. The MPE's were developed without considering objects with which the human may be in contact. Here the interaction of a human and a parasitically energized conductor is investigated. Rather than considering SAR, the specific interest is in whether or not the parasitically energized element can induce such large currents in the human that a burn will occur.

This problem is investigated using the finite-difference time-domain (FDTD) method. The conductor is a perfect electrically conducting (PEC) rod. The human is modeled using the standard "average man" ellipsoid. Although the FDTD method places almost no restrictions on the geometric complexity of an object (i.e., there is no computational savings provided by using a canonical shape such as an ellipsoid as opposed to a shape that more closely approximates that of an actual human), it was decided to use the standard ellipsoidal model. Since the interaction between the conductor and the human appears to be dominated by local effects, this geometric simplification should have only minor effects on the induced currents.

As will be shown, it is found that the parasitic element can cause a nearly one-thousand fold increase in the induced current in the ellipsoid compared to the current that exists when the conductor is not present. It is further noted that when a slight gap (5.00 mm) exists between the conductor and the ellipsoid, the induced current is significantly reduced relative to the case where the two are in contact.

In the following section we discuss the model of the problem as it exists in the continuous (real) world. Finally, results from the FDTD simulations are presented followed by some concluding comments.

Continuous World Model

In this section the problem as it exists in the continuous world (i.e., the "real" world) is described. A human was approximated using the "average man" ellipsoid model. The equation for the surface of an ellipsoid is

$$\frac{x^2}{a^2}+\frac{y^2}{b^2}+\frac{z^2}{c^2}=1 \qquad \textbf{(Equation 8)}$$

The "average man" model dictates that the following parameters be used for the ellipsoid

$$\begin{array}{ll} a = 0.098 \text{ m} & 2a = 0.196 \text{ m} \\ b = 0.195 \text{ m} & 2b = 0.390 \text{ m} \\ c = 0.875 \text{ m} & 2c = 1.750 \text{ m} \end{array} \qquad \textbf{(Equation 9)}$$

This ellipsoid will be referred to as the "man." The material parameters used for the man are[2]:

$$\varepsilon_r = 50.00 \qquad \textbf{(Equation 10)}$$

$$\mu_r = 1.00 \qquad \textbf{(Equation 11)}$$

$$\sigma = 1.0 \text{ S/m} \qquad \textbf{(Equation 12)}$$

Here, the effect the presence of a parasitic PEC rod has on the fields induced in the man will be examined. By parasitic, it is meant that the rod is not actively radiating. Of special interest is the current in the man adjacent to the contact point. The rod will be 2 m in length. The radius of the rod is dictated by the discretization used in the FDTD simulations (which will be described in more detail below). The rod will be aligned with the major axis of the ellipsoid, i.e., the z axis. When the rod is in contact with the top of the man, the total height of the man plus the rod is 3.75 m. Figure 3-1 shows a scale drawing of the "man" with the rod in contact with the top of the head. Here the origin is taken to be at the center of the man.

The excitation is a pulsed plane wave propagating in the x direction and polarized in the z direction. The pulse is a Ricker wavelet (i.e., the second derivative of a Gaussian pulse which is described in more detail in the Appendix). Spectral information is obtained from the time-domain FDTD simulation by taking the Fourier transform of the recorded fields and normalizing by the Fourier transform of the incident field.

Of special in interest is the current (or current density) that exists at a given point. This current can be obtained from the line integral of the magnetic field about a given point, i.e.,

[2] It is recognized that the dielectric properties of human tissue vary with frequency. In this work, the fixed values given above were used as a first approximation.

$$I_{enc} = \oint_L H \bullet dl \qquad \textbf{(Equation 13)}$$

where I_{enc} is the current enclosed in the path L.

FDTD Simulations

The FDTD method was used to perform the simulations. The FDTD method uses a discretization of both time and space, i.e., the fields are available only at discrete points in space and time. Within this discretized space-time, a time-marching scheme is used that solves a discrete form of Maxwell's equations. In order to understand fully the results that are to be presented, it is best to have a rudimentary understanding of the way in which the FDTD method approximates the continuous world.

For a Cartesian grid, such as is used in this study, one can think of the FDTD grid as consisting of a collection of small cubes where the components of the electric field exist on, and are parallel to, the edges of the cubes while the components of the magnetic field are centered on, and normal to, the faces of the cubes. Although one may use a non-uniform FDTD grid, here it is assumed the spatial step between nodes is the same in all directions, i.e., $\Delta_x = \Delta_y = \Delta_z = \delta$.

Within the grid, the ratio of the distance light can travel in one time step to the spatial step size is known as the Courant number given by $S_c = c\Delta_t/\delta$. (The ellipsoid dimensions not withstanding, c is always taken to refer to the speed of light in free space and here this is assumed to be 3×10^8 m/s). In order to obtain a stable simulation there is an inherent limit, known as the Courant limit, to the size of the Courant number. Throughout this study, the FDTD simulations will use a Courant number corresponding to the Courant limit of $1/\sqrt{3}$. (This value minimizes inherent numerical dispersion errors in the grid. Additionally, using the Courant limit ensures that a simulation proceeds as rapidly as possible since each update of the fields represents the greatest possible advance in time.)

In the simulations to follow, the spatial step size is $\delta = 5.00$ mm. The FDTD method also requires that one discretize some of the space surrounding the object(s) of interest. Here the grid is constructed so that there is at least 0.25 m between the man or rod and the start of the perfectly matched layer (PML) which is used to terminate the grid. Thus, the approximate overall size of the grid is 0.7 m x 0.9 m x 4.25 m.

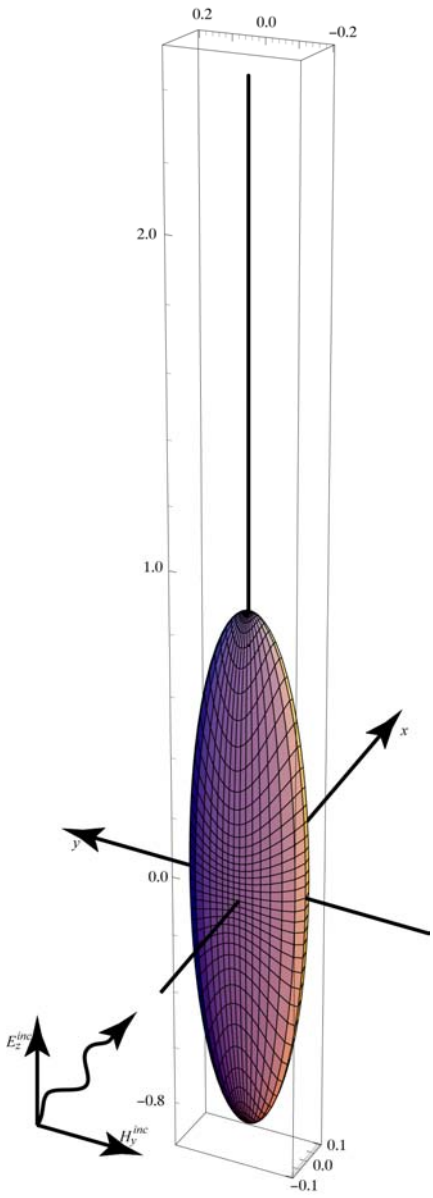

Figure 3-1
Scale drawing of the "average man" ellipsoid with a 2 m parasitic element in contact with the ellipsoid. The parasitic element is a PEC rod that is aligned with the major axis of the ellipsoid. The incident field is a z-polarized plane wave propagating in the x direction.

One of the important considerations when doing FDTD modeling is the number of points (or cells) per wavelength at a given frequency. The finer the discretization, i.e., the more points per wavelength, the smaller are the numerical artifacts in the results. (One can, in fact, show that the FDTD method is exact as the spatial step size goes to zero.) A general rule of thumb is that a discretization of 10 to 20 points per wavelength is sufficiently accurate. Thus, in the simulations to follow, results with a discretization coarser than 15 cells per wavelength will not be considered. Ignoring loss, the wavelength in the man is given by

$$\lambda_d = \frac{c}{f\sqrt{\varepsilon_r}} = \frac{\lambda_0}{\sqrt{\varepsilon_r}} = \frac{\lambda_0}{\sqrt{50}}$$ **(Equation 14)**

where λ_0 is the free space wavelength at frequency f. A discretization of 15 cells per wavelength and a spatial step size of 5.00 mm corresponds to a wavelength (in the man) of 0.075 m. Using this for λ_d in Equation 14 and solving for the frequency, it is found that

$$f_{max} = \frac{c}{\lambda_d\sqrt{\varepsilon_r}}$$ **(Equation 15)**

$$= \frac{3x10^8}{0.075\sqrt{50}}$$ **(Equation 16)**

$$= 565.69 \text{ MHz}$$ **(Equation 17)**

Thus, for this level of discretization at least 15 points per wavelength (in the man) will be maintained provided the frequency is no higher than 565.69 MHz. In free space, this corresponds to a sampling of approximately 106 points per wavelength.

A "stairstep" approximation of the ellipsoidal man will be used. In this approach the center of each cube in the grid is tested to see if it falls on or within the ellipsoid. If it does, the 12 electric field nodes on the edges of that cube are set to have the material parameters of the man.

The parasitic PEC rod is realized by setting to zero the E_z component of the electric field along a line extended along the major axis of the ellipsoid. A two-dimensional slice of the FDTD grid in the vicinity of the contact point between the rod and the man is depicted in Figure 3-2 (the curvature of the ellipsoid is not drawn to scale). One can picture this as either a constant-x plane or a constant-y plane. In either case, the vertical arrows represent the location of E_z nodes. If this were a constant-y plane, the horizontal arrows would correspond to E_x nodes while the dots would correspond to the location of H_y nodes (oriented orthogonal to the plane). If this were a constant-x plane, the horizontal arrows would correspond to E_y nodes while the dots would correspond to the location of H_x nodes (again, oriented orthogonal to the plane).

The thickness of the rod is slightly ambiguous. Since it is realized by zeroing a single line of E_z nodes, one can argue that its diameter is, at least approximately, equal to that of the spatial stepsize, i.e., δ = 5.00 mm. However, some FDTD studies of the behavior of this kind of "thin wire" rod have shown that the effective diameter is closer to that of 0.45 δ. Nevertheless, these studies were based on the behavior of the field in the radial direction away from the ends of the wire/rod. In this work, where specific interest is in the behavior at the end, this thickness is believed to be a secondary consideration.

The stair-stepped boundary shown in Figure 3-2 corresponds to the FDTD approximation of the outer surface of the man. Note that nodes that actually lie outside of the ellipsoid may,

nevertheless, be treated as being inside the man. The gray bar that begins above the ellipsoid corresponds to the PEC rod (the E_z nodes inside this bar are set to zero).

The current can be measured as given by Equation 13. However one must account for the discrete nature of the FDTD grid: instead of a continuous integral, one merely sums the magnetic fields over a given path (and multiplies the fields by the length over which they exist which is simply the spatial step size of δ). For example, assume one wishes to find the current flowing in the z direction in the man just below the contact with the rod. This essentially amounts to finding the current that exists at the location of the top-most E_z node in the ellipsoid. This top-most node is labeled E_z^0 in Figure 3-2. This current is found by summing (with appropriate sign changes) the four magnetic field nodes that swirl around the E_z^0 node, i.e., summing the two H_x and the two H_y nodes adjacent to E_z^0. Note that using this approach one can also calculate the current in the rod itself. Although E_z is zero in the rod, the magnetic fields adjacent to the rod are non-zero and can be used to obtain the current.

Since the FDTD method is a time-domain method, the current that one obtains directly from the FDTD simulation is in the time-domain, i.e., direct application of Equation 13 yields $I_{enc}(t)$. This "instantaneous" current is not of interest here. Instead, the interest is in the current at a given frequency that is induced by a unit-amplitude plane wave. To obtain this, one transforms the current to the frequency domain using a Fourier transform. Furthermore the fields must be normalized by the incident field. To do this, an auxiliary simulation is performed in which the incident field $E_z^{inc}(t)$ is recorded. The ellipsoid and the rod are removed from this simulation and the E_z field is recorded at a point that corresponds to the major axis of the ellipsoid. The frequency-domain current is then obtained by

$$I_{enc}(\omega) = \frac{F\left[I_{enc}(t)\right]}{F\left[E_z^{inc}(t)\right]} \qquad \textbf{(Equation 18)}$$

where F[ ] is the discrete Fourier transform.

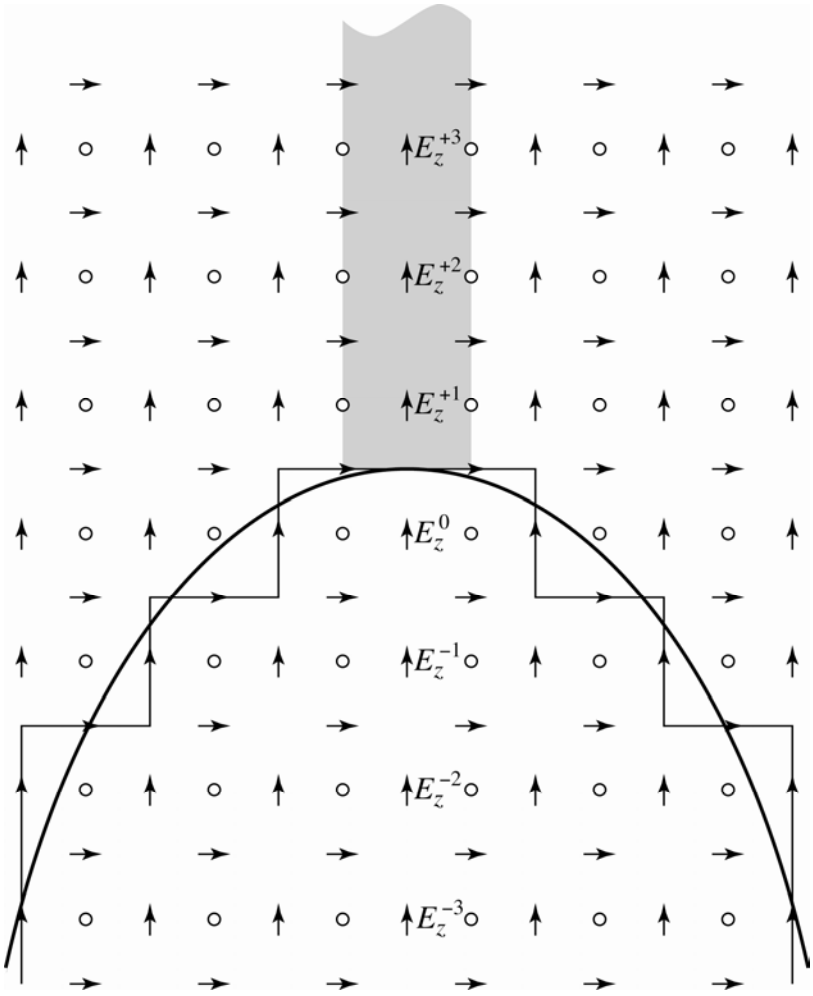

Figure 3-2
Depiction of the FDTD grid in the vicinity of the rod and ellipsoid contact-point. The labeled E_z nodes correspond to the locations where the current is measured.

The FDTD simulations were performed for 24576 time steps. After this number of time steps the fields in the computational domain were down by approximately 120 dB relative to their peak values. The temporal step size can be found from the Courant number and the spatial step size: $\Delta_t = S_c\delta/c = 9.6225$ ps. Given these values, the spectral resolution from the discrete Fourier transform is $\Delta f = 1/(24576\ \Delta_t) = 4.2287$ MHz.

Results

As shown in Figure 3-2, the fields from an FDTD simulation are recorded so that the current can be obtained at locations both above and below the top of the "man." The top-most point in the ellipsoid is labeled with a superscript "0." Points below this are labeled with a negative integer corresponding to the number of steps they are below the top-most point. Points above are labeled with a positive integer index ("+1" corresponds to the point just above the ellipsoid).

Three scenarios are considered:

1. A plane wave illuminating only the man. The parasitic element is not present.
2. A plane wave illuminating the man and the rod when the rod is in contact with the man (as indicated in Figures 3-1 and 3-2).
3. A plane wave illuminating the man and the rod when there is a 5.00 mm gap between the rod and the man. Referring to Figure 3-2, this would correspond to having the node E_z^{+1} be free space.

Before turning to the quantitative results, six "snapshots" taken from the three different simulations will be shown. These snapshots serve to illustrate important qualitative differences in the behavior of these different scenarios. The snapshots show color maps of the E_z -component of the electric field in the vicinity of the top of the ellipsoid. The field is recorded over either a constant-x or a constant-y plane that passes through the center of the computational domain (and hence passes through the parasitic rod when it is present). The snapshots are taken over only a portion of the entire computational domain and are taken at three different time-steps: 1400, 1700, and 2000. For the particular excitation that is used (which is discussed in further detail in the Appendix), timestep 1700 is close to when the peak current exists at the top of the man when the rod is present.

Figure 3-3 shows the snapshots when the man is present but the parasitic rod is not. The images along the left side of the page depict the E_z field over constant-x planes that pass through the center of the man. Since the incident field is a plane wave propagating in the x direction, these images are symmetric about the major axis of the ellipsoid. The images along the right side of the page show the E_z field over constant-y planes. In these images the incident plane wave is propagating left-to-right. Pairs of images (i.e., (a) and (b); (c) and (d); and (e) and (f)) were recorded at the same time.

These color maps, and the ones shown in the following two figures, use logarithmic scaling, meaning that the fields are visible, at least to some degree, over a logarithmic scale. In this particular case the scaling was chosen so that the fields are visible over three orders of magnitude. The maximum field was normalized to a value of 5.0 V/m. In the color-bar shown along the right-hand side of each pair of images, the color at the top of the bar corresponds to 5.0 V/m. One may think of this as the "zero value" meaning the field corresponds to the normalized value of 5.0×10^{0} V/m. The color labeled "−1" in this bar corresponds to 5.0×10^{-1} V/m while the one labeled "−2" corresponds to 5.0×10^{-2} V/m. The bottom of the bar corresponds to values that are at, or below, 5.0×10^{-3} V/m. As described in the Appendix, the incident pulse has a peak amplitude of 1.0 V/m.

In Figure 3-3 one observes a rather pronounced difference in the field magnitude in free space relative to the field within the man. As one might expect for this incident field (which is polarized along the major axis of the ellipsoid) and for the dimensions of this particular ellipsoid (where the aspect ratio is nearly 9-to-1 between the c and a dimensions), the field can be relatively strong at the top of the ellipsoid. (Since this ellipsoid is in free space, the same fields

exist at the bottom.) However, the snapshots show that the fields do not build up to a large value within the man. Note that at the very top of the ellipsoid the z component of the electric field is normal to the interface and normal components of field, unlike tangential components, need not be continuous across a boundary. The lack of penetration of the field into the man is not unexpected given the large mismatch between the characteristic impedance of the man and free space. Ignoring loss for a moment, the characteristic impedance of the man is $\eta_0/\sqrt{50}$ where η_0 is the characteristic impedance of free space. The magnitude of the reflection coefficient for a plane wave normally incident from free space onto a material with an impedance of $\eta_0/\sqrt{50}$ is approximately 0.752. When one includes loss of σ = 1.00 S/m, such as the case here, the magnitude of the reflection coefficient increases, e.g., at 100 MHz the magnitude of the reflection coefficient is approximately 0.89.

In Figure 3-3 one can see some relative "hot spots" along the surface of the man. These are caused by the stairstep approximation to the continuous surface. As such, these are numerical artifacts, but relatively minor ones—they do not lead to large fields inside the man nor do they cause any significant perturbation of the field as one moves away from the surface.

Figure 3-4 shows the E_z field recorded at the same times and over the same locations as shown in Figure 3-3. However, in these snapshots the parasitic rod is present. Since E_z is zero in the rod and the observation planes pass through the rod, in these snapshots the location of the rod corresponds to the black line that is centered horizontally and starts at the top of the man.

The presence of the rod affects the fields both in and around the man—it changes the overall resonance of the system. In these snapshots it appears the fields external to the man have been reduced in some regions. That is indeed the case. However, our focus is more on the effect the rod has on the field (or current) within the man. In Figure 3-3(c)–(d), if one looks closely at the top of the man, there are clearly "red" regions where none existed before. One should note that the red is fairly well localized to the region in the vicinity of the contact point. Furthermore, the field appears to decay in a manner that is consistent with spherical spreading, i.e., there is no apparent concentration of the field at the surface of the ellipsoid or along the major axis (the axis of symmetry). Given the homogeneity of the ellipsoid, such a result is not unexpected.

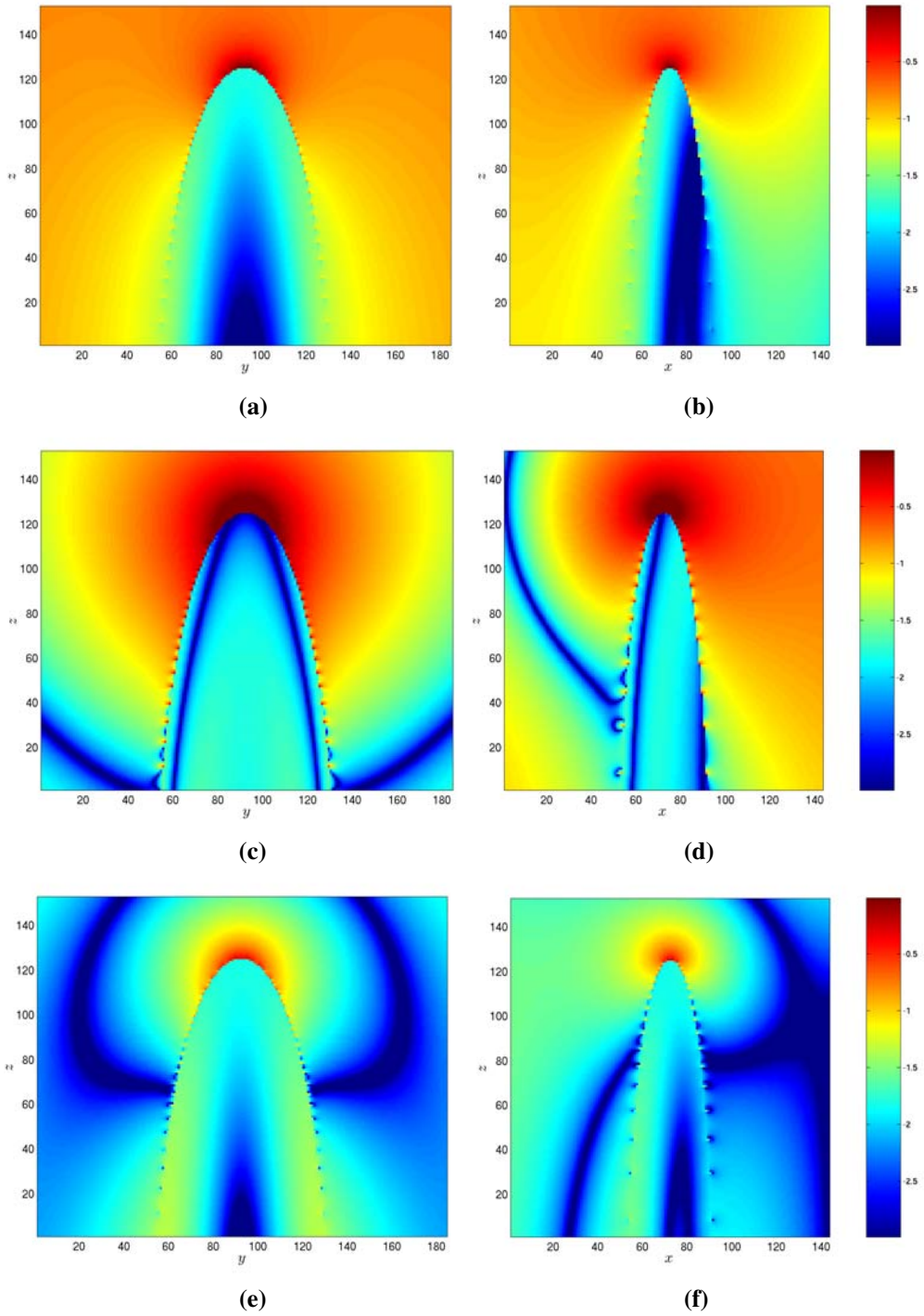

Figure 3-3
Color map of the log (E_z) field in the vicinity of the top of the man at three different times. The rod is not present. Images in the left column ((a), (c), and (e)) show the field over a constant-x plane while images in the right column ((b), (d), and (f)) show the field over a constant-y plane. (a) and (b) correspond to time-step 1400. (c) and (d) correspond to time-step 1700. (e) and (f) correspond to time-step 2000.

The snapshots for the third scenario, in which there is a 5.00 mm gap between the rod and the man, are shown in Figure 3-5. These snapshots depict the E_z field at the same times and over the same space as those of the previous two figures. Inspecting the top of the man, one sees that the field is more intense than when there is no rod, but there are no "red hot" nodes. Thus, it appears that even as slight a gap as 5.00 mm may greatly reduce the current induced in the man (although one should keep in mind that so far only fields, not currents have been examined).

These same three scenarios are now revisited and the current that flows in the seven labeled nodes shown in Figure 3-2 is plotted. Figure 3-6 shows the currents that exist when the rod is not present. In this plot and the following plots, the current at the top-most node in the man will be plotted as a solid red line. The current at the three nodes below this are also plotted as solid lines. The currents for the nodes above the ellipsoid are plotted with symbols or a dashed line. Recall that there is no distinction being made between conduction current (σE) and displacement current ($\varepsilon \partial E/\partial t$)—Equations 13 and 18 yield total current. Thus it is perfectly reasonable to have a current that exists in free space.

Owing to the conductivity in the man and the greater permittivity, Figure 3-6 shows that for any given frequency the current at the sample points in the man exceeds that found in the points above the man. Below about 200 MHz there is very little difference in the current that is found in the points in the man. Note that the current is plotted in milliamperes and remains small over this entire band of frequencies (i.e., less than 15 μA).

The currents that exist when the rod is in contact with the top of the man are shown in Figures 3-7 and 3-8. Figure 3-7 shows the current for the nodes within the man while Figure 3-8 shows the currents in the top-most node in the man and the three nodes directly above the man (i.e., the three nodes in the bottom of the rod). One should note when comparing Figure 3-6 and Figure 3-7 that the current in the top-most node increases by a factor of nearly a thousand when the rod is present. One can also see from Figure 3-7 that the current decays rather rapidly away from the top-most node (e.g., decaying by over a factor of three from the top-most node to the adjacent node). Figure 3-8 shows that over this range of frequencies there is very little spatial variation in the current at the end of the rod. It can also be seen that the current at the end of the rod is slightly more than four times greater than the current in the top-most node in the man. (One may be inclined to ask where the current "went" between the end of the rod and the top of the man. Note there are four nodes, two E_x and two E_y nodes, that are between and orthogonal to the E_z node at the top of the man and the E_z at the bottom of the rod. If one assumes the current must be conserved, then at 40 MHz these four nodes would each carry roughly 8 mA of current to account for the total current flowing at the end of the rod.)

Finally, Figures 3-9 and 3-10 show the currents that exist at these same observations points when there is a gap of 5.00 mm between the rod and the man. Figure 3-9 shows the current in the nodes within the man while Figure 3-10 shows the currents at the top-most node in the man and the three nodes above that. In this case the current labeled E_z^{+1} is in free space while E_z^{+2} and E_z^{+3} are in the rod. Although the currents in the man are greater than when the rod is not present, this small gap makes a rather dramatic reduction in the amount of current that flows in the top-most node, reducing the current by a factor of nearly 60 compared to when there is no gap. It can also

be observed that the fields do not decay quite as rapidly away from the top. Going from the top-most node to the adjacent node yields a reduction in the current by a factor of about 1.7 as opposed to a reduction by a factor of nearly 3 when the rod is present.

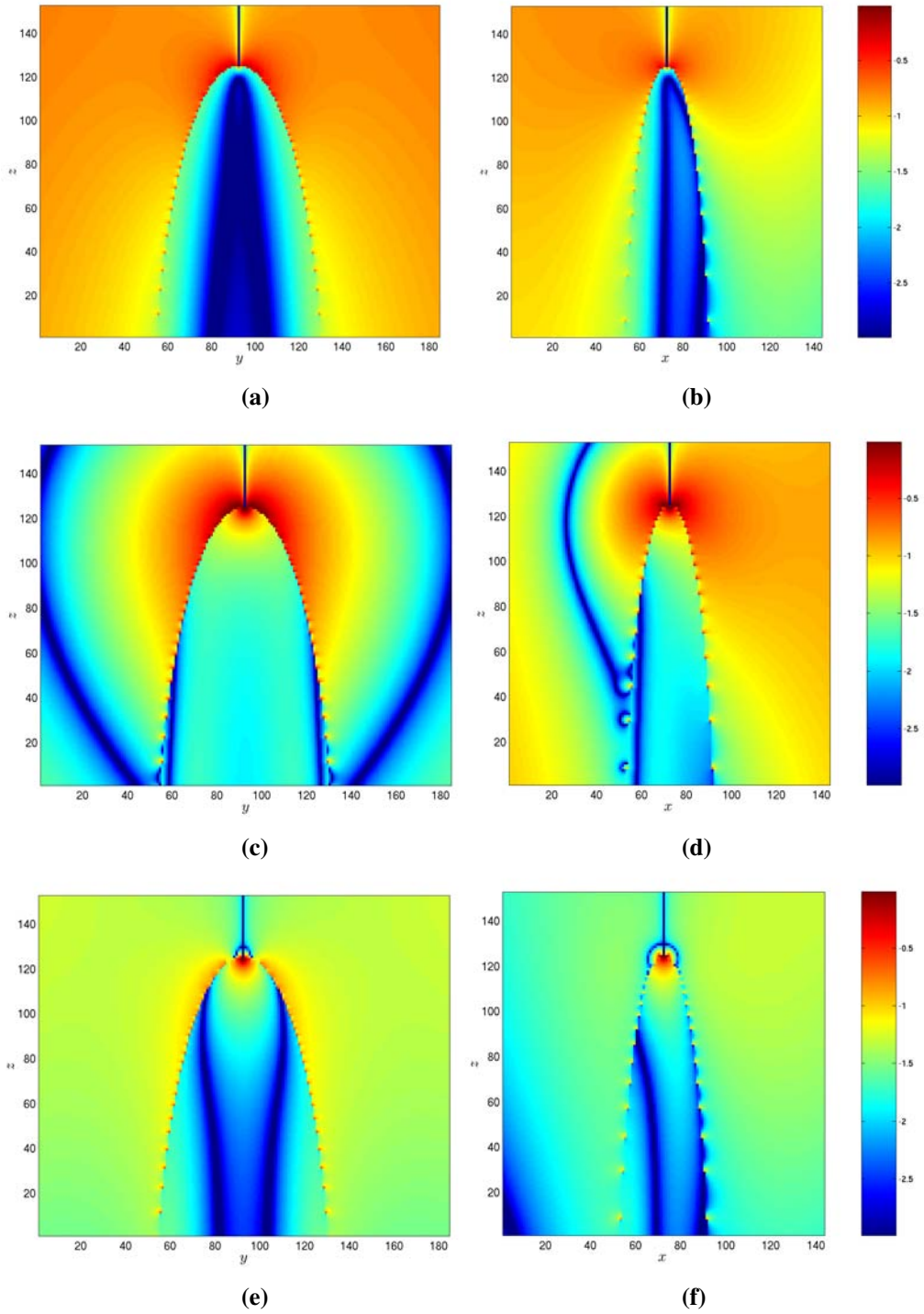

Figure 3-4
Color map of the log (E_z) field recorded at the same time-steps and locations as in Figure 3-3. However, unlike Figure 3-3, now the parasitic rod is present and in contact with the man. Since E_z is zero within the rod, the rod appears as a black line in each image.

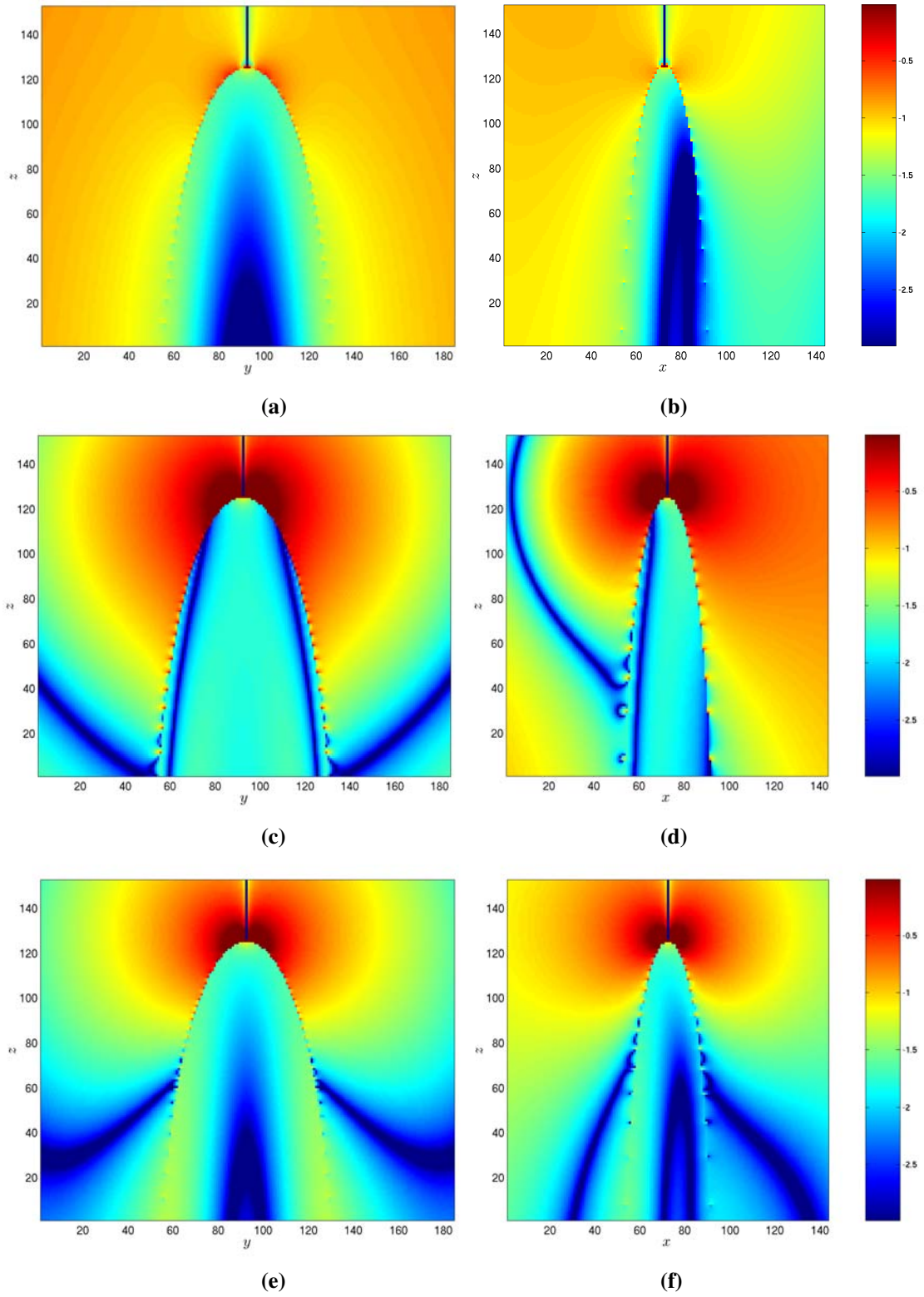

Figure 3-5
Color map of the log (E_z) field recorded at the same time-steps and locations as in Figure 3-3. The rod is present but there is a single-cell gap (5.00 mm) between the end of the rod and the top of the man.

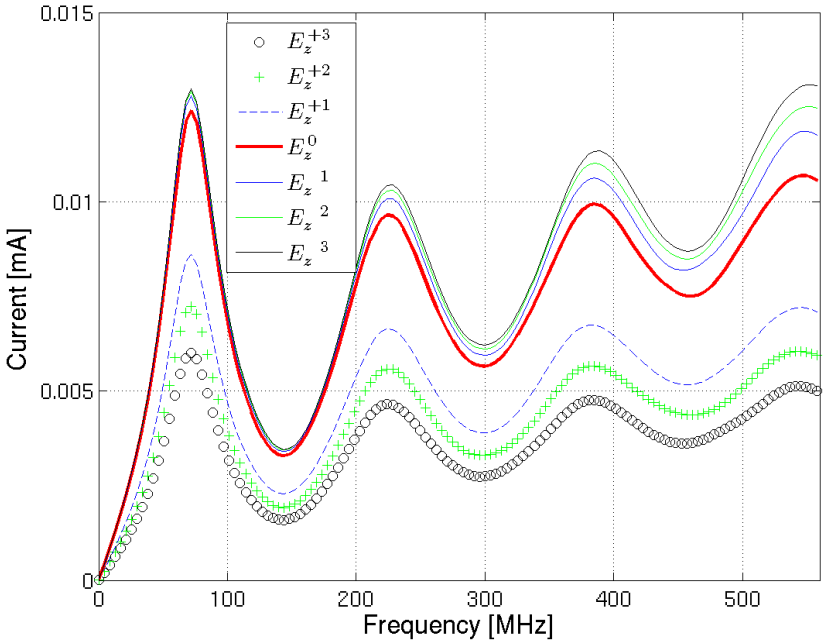

Figure 3-6
Currents (rms) at the seven nodes along the major axis of the ellipsoid in the neighborhood of the top of the ellipsoid. The labels in the legend correspond to the nodes shown in Figure 3-2. Solid lines are used for locations within the ellipsoid while symbols or a dashed line correspond to locations above the ellipsoid. The incident electric field is 1 V/m rms.

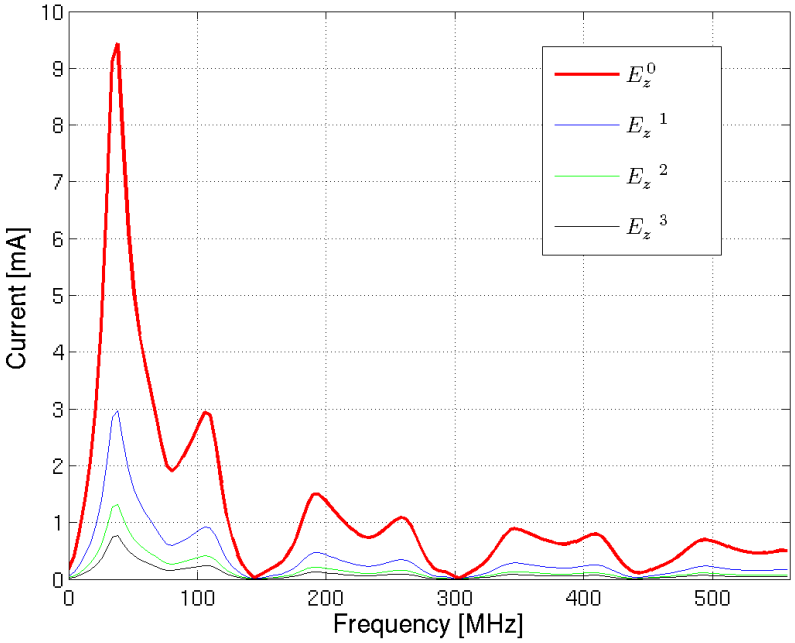

Figure 3-7
Currents (rms) at the nodes within the man when the rod is in contact with the man. The incident electric field is 1 V/m rms.

Conclusions

Using FDTD simulations where a man is approximated by the "average man" ellipsoid, it was observed that having a parasitic element in contact with the man can have a rather dramatic effect on the amount of current induced by exposure to an electromagnetic field: The induced current increases by a factor of nearly one thousand relative to when the parasitic element is not present. The parasitic element was a PEC rod aligned with the major axis of the ellipsoid. The incident field was a plane wave polarized in the direction of the major axis of the ellipsoid (and hence aligned with the rod).

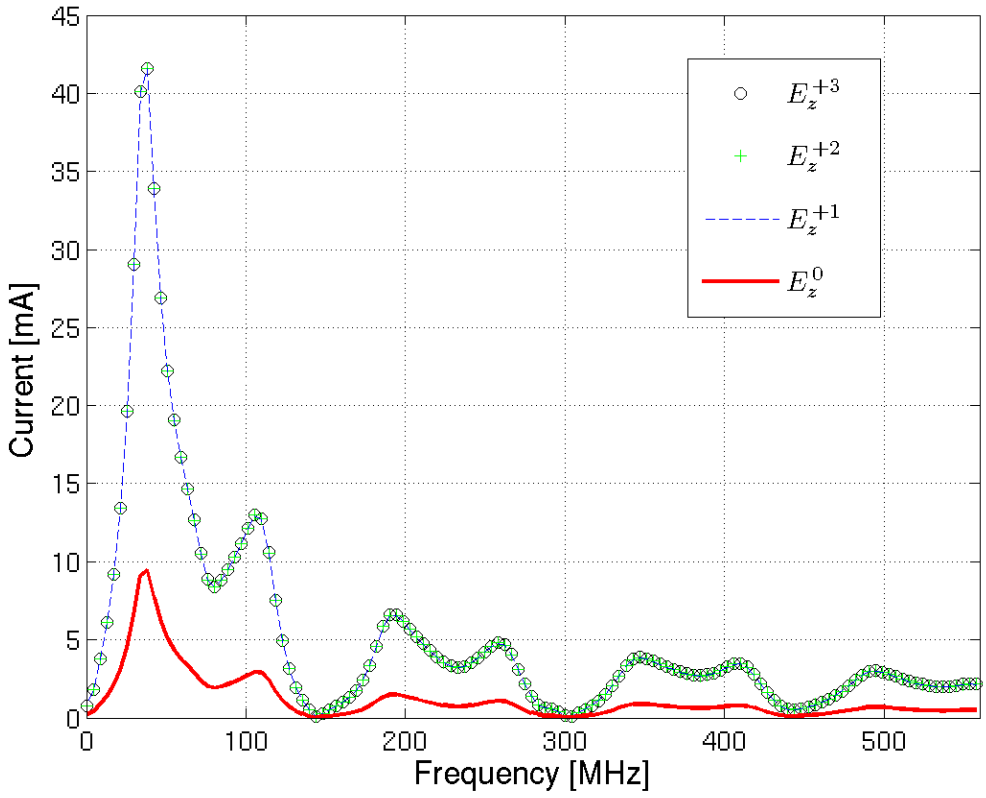

Figure 3-8
Currents (rms) at the top-most node in the man and the three nodes above the man. The nodes outside the man are all within the rod and have nearly the same amount of current. The incident electric field is 1 V/m rms.

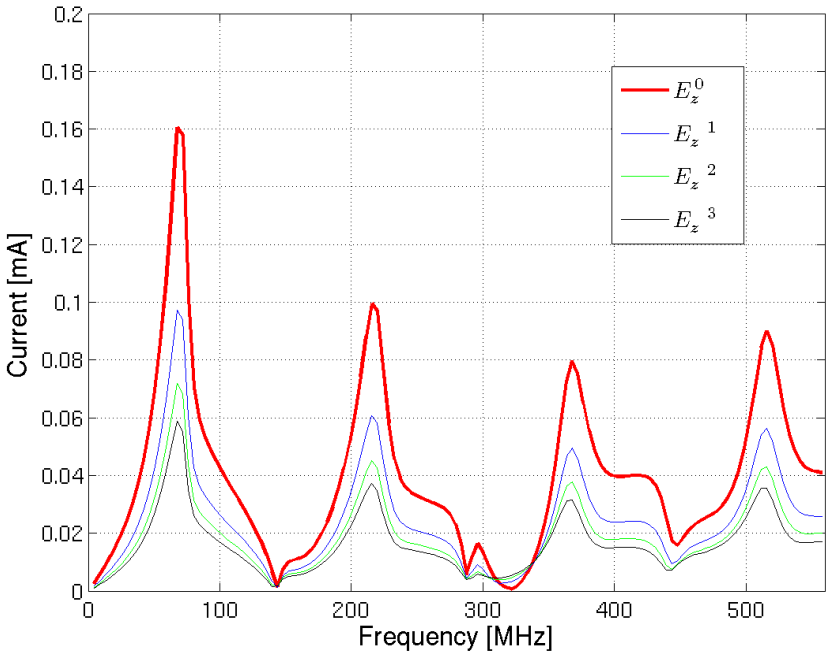

Figure 3-9
Currents (rms) when the rod is separated from the man by 5.00 mm. The observation points are the four highest nodes in the man. The incident electric field is 1 V/m rms.

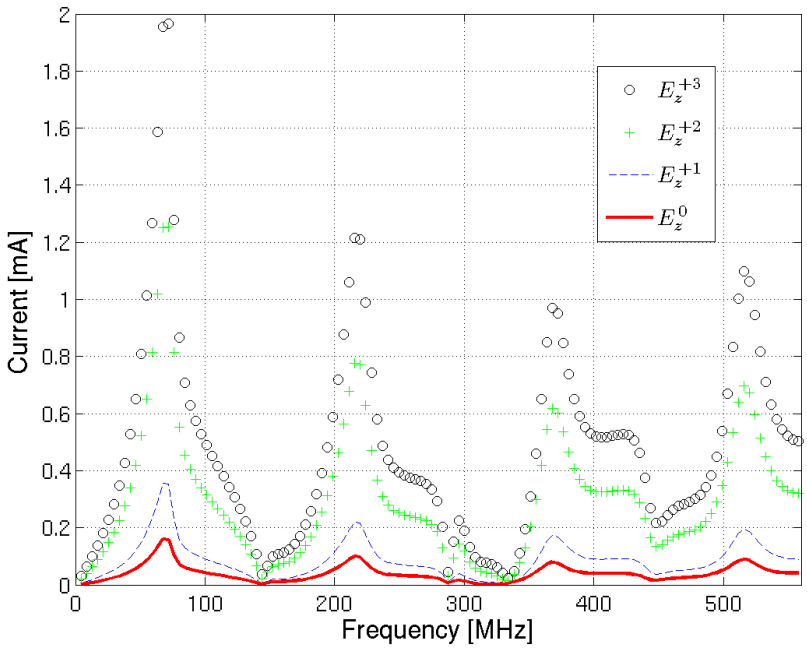

Figure 3-10
Currents (rms) when the rod is separated from the man by 5.00 mm. The observation points are the top-most point in the man and the three nodes above the man. The incident electric field is 1 V/m rms.

It was further observed that introduction of a slight gap (5.00 mm) between the rod and the man caused a significant reduction in the current relative to when the two were in contact. (The factor by which the current was reduced was on the order of 60.) The effects of having the parasitic element in contact with the man appear to be rather localized, consistent with spherical spreading of the field away from the contact point.

Clearly, from Figure 5-7, the current induced in a human model by contact with an indirectly energized rod is smaller as frequency increases. This would indicate that the MPE limits are more likely to be protective against RF burns at higher frequencies. At 110 MHz, however, the amount of current passing from the conductor into the human when the two are in contact is in the range of currents believed sufficient to cause a burn. The threshold of the current needed to cause a burn is thought to be in the 10 - 100.0 mA range for contact areas of 0.05 cm^2 (i.e., a current density of between 200 - 2000 mA/cm^2). For an incident electric field of 61.4 V/m rms (i.e., the MPE occupational limit from 30 – 300 MHz) the maximum induced current at 110 MHz from Figure 5-7 would be 184 mA (i.e., contact current of 3 mA x 61.4 since the incident field was assumed to be 1 V/m in this analysis). Since the contact area in the FDTD model is approximately 0.25 cm^2 the current density in this case would be approximately 736 mA/cm^2, in the range of current densities that might cause an RF burn. More information is needed about the appropriate method to relate threshold current and contact area before a more definitive conclusion can be made.

It is not clear if simulations were done with even a finer discretization if one would find a significant change in either the total current or the current density. (It has been observed, when using a finer discretization, that the current does increase as one moves closer to the contact point.) The results presented here were obtained using the finest discretization possible given our in-house computational resources.

Finally, it can be noted that when the rod is present the induced current is seen always to be greatest at the lowest resonant frequency of the system. Thus, it appears if guidelines were to be developed to be protective of exposure to parasitic elements, those guidelines could be developed by considering the behavior at the lowest resonance.

4
REFERENCES

Absten, G. T. (2002). Practical Electrosurgery for Clinicians. Professional Medical Education Association, Inc., PO Box 522379, Marathon Shores, FL 33052. www.lasertraining.org. http://www.lasertraining.org/Administrative/Library/Practical%20Electrosurgery%20Manual.pdf

Agarwal, K., A.-C. Lange and H. Beck (2007). Thermal imaging in healthy humans – What is "normal" skin temperature? InfraMation 2007 Proceedings, Infrared Training Center Document 121A 2007-05-04. ITC Americas, Boston, 16 Esquire Road, N. Billerica, MA 01862. http://itcnewsletter.com/

Chatterjee, I., D. Wu and O. P. Gandhi (1986). Human body impedance and threshold currents for perception and pain for contact hazard analysis in the VLF-MF band. IEEE Transactions on Biomedical Engineering, Vol. BME-33, No. 5, May, pp. 486-494.

Chatterjee, I., Y. Gu and O. P. Gandhi (1986). Quantification of electromagnetic absorption in humans from body-mounted communications transceivers. IEEE Transactions on Vehicular Technology, Vol. VT-34, No. 2, pp. 55-62.

Chen, J.-Y. and O. P. Gandhi (1988). Thermal implications of high SARs in the extremities at the ANSI-recommended MF-VHF safety levels. IEEE Transactions on Biomedical Engineering, Vol, 35, Issue 6, pp. 435-441.

Ciano, M., J. Burlin, R. Pardoe, R. Mills and V. Hentz (1981). High-frequency electromagnetic radiation injury to the upper extremity: local and systemic effects. Annals of Plastic Surgery, Vol. 7, No. 2, pp. 128-135.

Dewhirst, M. W., B. L. Viglianti, M. Lora-Michiels, M. Hanson and P. J. Hoopes (2003). Basic principles of thermal dosimetry and thermal thresholds for tissue damage from hyperthermia. International Journal of Hyperthermia, Vol. 19, No. 3 (May-June 2003), pp. 267-294.

EPRI (2008). Radiofrequency Burns in the Workplace. EPRI, Palo Alto, CA. 1015627

Gandhi, O.P., I. Chatterjee, D. Wu and Y-G Gu (1985). Likelihood of high rates of energy deposition in the human legs at the ANSI recommended 3-30 MHz RF safety levels. Proceedings of the IEEE, Vol. 73, No. 6, pp. 1145-1147.

Gandhi, O.P., J.-Y. Chen and A. Riazi (1986). Currents induced in a human being for plane-wave exposure conditions 0-50 MHz and for RF sealers. IEEE Transactions on Biomedical Engineering, Vol. BME-33, August, pp. 757-767.

Guy, A. W. and C.-K. Chou (1987). Data analysis of VLF hazards study. Final report on contract no. A-3529-160-S1 prepared for Engineering Experimental Station, Georgia Institute of Technology by Bioelectromagnetics Research Laboratory, University of Washington.

Hocking B., K. J. Joyner, H. H. Newman and R. J. Aldred (1994). Radiofrequency electric shock and burn. The Medical Journal of Australia, Vol. 161, No. 5/19, December, pp. 683-685.

Hocking, B. and R. Westerman (1999). Radiofrequency electrocution. Occupational Medicine, Vol. 49, No.7, pp. 459-461.

IEEE (1999). IEEE Standard Safety Levels with Respect to Human Exposure to Radio Frequency Electromagnetic Fields, 3 kHz to 300 GHz. IEEE Std C95.1, 1999 Edition (Incorporating IEEE Std C95.1-1991 and IEEE Std C95.1a-1998). The Institute of Electrical and Electronics Engineers, Inc., 345 East 47th Street, New York, NY 10017-2394.

IEEE (2005). IEEE Standard Safety Levels with Respect to Human Exposure to Radio Frequency Electromagnetic Fields, 3 kHz to 300 GHz. IEEE Std C95.1-2005 (Revision of IEEE Std C95.1-1991). The Institute of Electrical and Electronics Engineers, Inc., 345 East 47th Street, New York, NY 10017-2394.

ICNIRP (1998). (International Commission on Non-Ionizing Radiation Protection), "Guidelines for limiting exposure to time-varying electric, magnetic, and electromagnetic fields (up to 300 GHz)," Health Physics, vol. 74, pp. 494–522, 1998.

Moon, J. K. (2006). Warmed blankets are safe. Publication E114 (February). Enthermics Medical Systems. W164N9221 Water Street, Menomonee Falls, WI 53051. www.enthermics.com

Moritz A. and F. Henriques (1947). Studies of thermal injury II. The relative importance of time and surface temperature in the causation of thermal burns. American Journal of Pathology, Vol. 23,pp. 695-720.

Navy (1982). Electromagnetic Radiation Hazards (U) (Hazards to Personnel, Fuel and Other Flammable Material) (U). Technical Manual. NAVSEA OP 3565/NAVAIR 16-1-529 Volume 1, Sixth Revision. Naval Sea Systems Command, February.

Navy (1973). Radio Frequency Burn Hazards Reduction. Technical Manual, NAVSHIPS 0967-317-7010 (First Revision). Department of the Navy, Naval Ship Engineering Center, January.

Olsen, R. G., T. A. Griner, B. J. Van Matre and J. J. King (1994). Measurements of Radiofrequency (RF) Body Potential and Body Current in Personnel Aboard Two Classes of

Navy Ships. Naval Aeromedical Research Laboratory report 1384. AD-A275-760 (Defense Technical Information Center http://www.dtic.mil/dtic/.

Pearce, J. A., L. A. Gesses, J. F. Van Vleet, K. Foster and J. Allen (1983). Skin burns from electrosurgical current. Medical Instrumentation, Vol. 18, No. 3, May-June, pp. 225-231.

Reilly J. P. (1998). Applied Bioelectricity: From Electrical Stimulation To Electropathology, Springer, NY, 1998.

Rogers, S. J. (1981). In Proceedings of a Workshop on the Protection of Personnel Against Radiofrequency Electromagnetic Radiation (J. C. Mitchell, ed.). Radiofrequency burn hazards in the MF/HF band. Review 3-81, USAC School of Aerospace Medicine, Brooks, Air Force Base, TX 78235.

Slade, P. G. (ed) (1999). Electrical Contacts Principles and Applications. Marcel Dekker, Inc., 270 Madison Avenue, New York, NY 10016. ISBN 0-8247-1934-4.

Stoll, A. and L. Greene (1959). Relationship between pain and tissue damage due to thermal radiation. Journal of Applied Physiology, Vol. 14, pp. 373-382.

Tell, R. A. (1993). RF Current Reduction Provided by Work Gloves at AM Radio Broadcast Frequencies. Technical report prepared for the Federal Communications Commission, Office of Engineering and Technology, Washington, DC, FCC/OET RTA 93-01 [NTIS order no. PB94-117041].

A
APPENDIX

Source Function: Ricker Wavelet

One of the features of the FDTD technique is that it allows the modeling of a broad range of frequencies using a single simulation. Therefore, when possible, it is generally advantageous to use pulsed sources—which can introduce a wide spectrum—rather than a harmonic source. In the simulations presented here, the source function is a Ricker wavelet. A Ricker wavelet is equivalent to the second derivative of a Gaussian; it is simple to implement; it has no dc component; and, its spectral content is fixed by a single parameter. In the continuous world the Ricker wavelet is often written

$$f_r(t) = \left(1 - 2\left\{\pi f_p \left|t - d_r\right|\right\}^2\right) \exp\left(-\left\{\pi f_p \left|t - d_r\right|\right\}^2\right) \qquad \textbf{(Equation 19)}$$

where f_p is the "peak frequency" and d_r is the temporal delay. As will be more clear when the spectral representation of the function is shown below, the peak frequency is the frequency with the greatest spectral content.

The delay d_r can be set to any desired amount, but it is convenient to express it as a multiple of $1/f_p$, i.e.,

$$d_r = M_d \frac{1}{f_p} \qquad \textbf{(Equation 20)}$$

where M_d is the delay multiple (which need not be an integer). An FDTD simulation is typically assumed to start at t = 0, but $f_r(t)$ is not zero for $t < 0$—rather $f_r(t)$ asymptotically approaches zero for large and small values of the argument, but never actually reaches zero (other than at two discrete zero-crossings). However, with a delay of $d_r = 1/f_p$ (i.e., $M_d = 1$), $|f_r(t < 0)|$ is bound by 0.001, which is small compared to the peak value of unity. Thus, the transient caused by "switching on" $f_r(t)$ at t = 0 is relatively small with this amount of delay. Said another way, since the magnitude of $f_r(t)$ is small for $t < 0$, these values can be approximated by assuming they are zero. Here the delay multiple was set to unity.

The Fourier transform of Equation 19 is

$$F_r(\omega) = -\frac{2}{f_p\sqrt{\pi}}\left(\frac{\omega}{2\pi f_p}\right)^2 \exp\left(-jd_r\omega - \left[\frac{\omega}{2\pi f_p}\right]^2\right) \qquad \textbf{(Equation 21)}$$

Note that the delay d_r only appears as the imaginary part of the exponent. Thus it affects only the phase of $F_r(\omega)$, not the magnitude. The functions $f_r(t)$ and $|F_r(\omega)|$ are shown in Figure 3-11. For the sake of illustration, f_p is arbitrarily chosen to be 1 Hz and the delay is 1 s. Different values of f_p change the horizontal scale but they do not change the general shape of the curve. To obtain unit amplitude at the peak frequency, $F_r(\omega)$ has been scaled by $f_p e\sqrt{\pi}/2$.

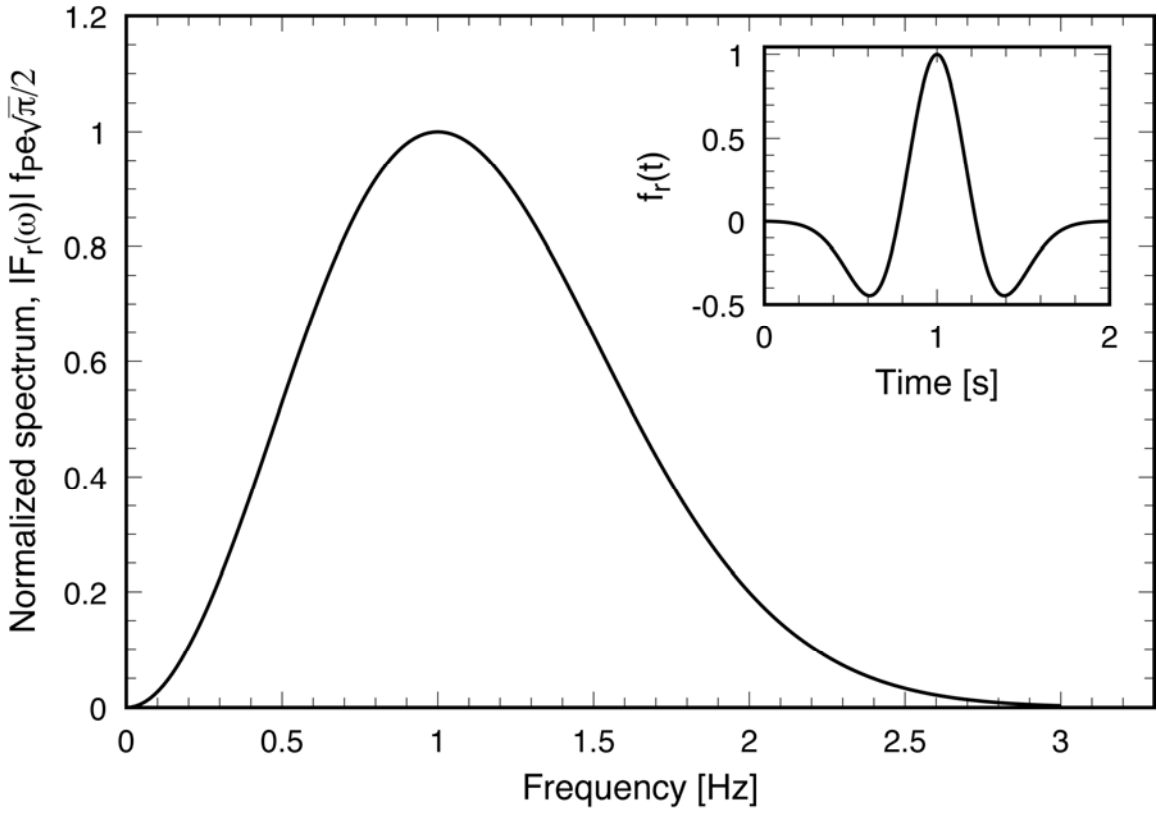

Figure A-1
Normalized spectrum of the Ricker wavelet with f_p = 1 Hz. The corresponding temporal form $f_r(t)$ is shown in the inset box where a delay of 1 s has been assumed. For other values of f_p , the horizontal axis in the time domain is scaled by $1/f_p$. For example, if f_p were 1 MHz, the peak would occur at 1 µs rather than at 1 s. In the spectral domain, the horizontal axis is directly scaled by f_p so that if f_p were 1 MHz, the peak would occur at 1 MHz.

The peak frequency f_p has a corresponding wavelength λ_p . This wavelength can be expressed in terms of the spatial step such that $\lambda_p = N_p\delta$, where N_p does not need to be an integer. Thus

$$f_p = \frac{c}{\lambda_p} = \frac{c}{N_p \delta}$$

(Equation 22)

The Courant number S_c is $c\Delta_t/\delta$ so the spatial step can be expressed as $\delta = c\Delta_t/S_c$. Using this in Equation 22 yields

$$f_p = \frac{S_c}{N_p \Delta_t}$$

(Equation 23)

The delay can thus be expressed as

$$d_r = M_d \frac{1}{f_p} = M_d \frac{N_p \Delta_t}{S_c}$$

(Equation 24)

Letting time t be $q\Delta_t$ and expressing f_p and d_r as in Equation 23 and Equation 24, the discrete form of Equation 19 can be written as

$$f_r(q) = \left(1 - 2\pi^2 \left\{\frac{S_c q}{N_p} - M_d\right\}^2\right) \exp\left(-\pi^2 \left\{\frac{S_c q}{Np} - M_d\right\}^2\right)$$

(Equation 25)

Note that the parameters that specify $f_r[q]$ are the Courant number S_c , the points per wavelength at the peak frequency N_p, and the delay multiple M_d there is no Δ_t in Equation 25. This function appears to be independent of the temporal and spatial steps, but it does depend on their ratio via the Courant number S_c. In the simulations performed here, the peak frequency was discretized at 720 points per wavelength in free space (this corresponds to a discretization of approximately 101 points per wavelength in the man).

Miscellaneous Details of the FDTD Simulations

The incident plane wave was introduced over a total-field/scattered-field (TFSF) boundary. This boundary separates the grid into an interior region, in which the ellipsoid and rod are enclosed, and an exterior region. The interior region contains the total field, i.e., the incident plus any scattered field, while the exterior region contains only scattered fields. In this work the only concern is the total field. (The snapshots shown in Figures 3-3 to 3-5 showed only the total-field region.)

To realize a TFSF boundary, one must know the incident field at every node that is tangential to and adjacent to the boundary. Because the incident field is propagating along one of the grid axes, the incident field is calculated using an auxiliary 1D simulation. This auxiliary simulation is simply modeling the free space propagation of a plane wave. Rather importantly, the way in which this incident field propagates in the auxiliary grid is exactly how it propagates in the 3D grid. Owing to the slight difference between the way waves propagate in the continuous world

and the way they propagate in the FDTD grid, this exact agreement would not be the case if one used the continuous-world expression to calculate the incident field at the nodes adjacent to the boundary.

The FDTD grid was terminated using the complex frequency-shifted perfectly matched layer (CPML) employing recursive convolution. The layer was eight cells thick. Previous studies conducted of problems with a long rod indicated that the CPML parameter α_{max} should be set to approximately 0.01 to minimize reflections from the grid. (This parameter affects the ability of the layer to absorb evanescent waves.) The FDTD code was written in such a way that it could be distributed over multiple processors. One of the limiting constraints in any large FDTD simulation is the amount of memory that can be used to discretize the computation space. Our code was written using the Message Passing Interface (MPI) library. In theory, this allows the simulation to run on any number of processors. In practice, because of network latency and communication overhead, there comes a point of diminishing return so that additional processors do not significantly reduce computation time. Our simulations were run on an in-house cluster of three nodes, each of which had two processors. Thus, the computational domain was sliced into six domains where the slices were along the z axis—each processor handled one of these domains. Counting from the bottom of the z axis, the snapshots shown in Figures 3-3 to 3-5 were of the E_z computed by the third processor.

Export Control Restrictions

Access to and use of EPRI Intellectual Property is granted with the specific understanding and requirement that responsibility for ensuring full compliance with all applicable U.S. and foreign export laws and regulations is being undertaken by you and your company. This includes an obligation to ensure that any individual receiving access hereunder who is not a U.S. citizen or permanent U.S. resident is permitted access under applicable U.S. and foreign export laws and regulations. In the event you are uncertain whether you or your company may lawfully obtain access to this EPRI Intellectual Property, you acknowledge that it is your obligation to consult with your company's legal counsel to determine whether this access is lawful. Although EPRI may make available on a case-by-case basis an informal assessment of the applicable U.S. export classification for specific EPRI Intellectual Property, you and your company acknowledge that this assessment is solely for informational purposes and not for reliance purposes. You and your company acknowledge that it is still the obligation of you and your company to make your own assessment of the applicable U.S. export classification and ensure compliance accordingly. You and your company understand and acknowledge your obligations to make a prompt report to EPRI and the appropriate authorities regarding any access to or use of EPRI Intellectual Property hereunder that may be in violation of applicable U.S. or foreign export laws or regulations.

The Electric Power Research Institute, Inc. (EPRI, www.epri.com) conducts research and development relating to the generation, delivery and use of electricity for the benefit of the public. An independent, nonprofit organization, EPRI brings together its scientists and engineers as well as experts from academia and industry to help address challenges in electricity, including reliability, efficiency, health, safety and the environment. EPRI also provides technology, policy and economic analyses to drive long-range research and development planning, and supports research in emerging technologies. EPRI's members represent more than 90 percent of the electricity generated and delivered in the United States, and international participation extends to 40 countries. EPRI's principal offices and laboratories are located in Palo Alto, Calif.; Charlotte, N.C.; Knoxville, Tenn.; and Lenox, Mass.

Together…Shaping the Future of Electricity

Program:

EMF Health Assessment and Radio-Frequency Safety

1017991

Electric Power Research Institute
3420 Hillview Avenue, Palo Alto, California 94304-1338 • PO Box 10412, Palo Alto, California 94303-0813 USA
800.313.3774 • 650.855.2121 • askepri@epri.com • www.epri.com